Controlling XUV's Harmonics Using Double IR Laser Pulses

By: Gideon Kiprono Korir

Supervisor: Prof. Anatole Kenfack

A thesis submitted in fulfillment of the requirements for Masters Degree in Theoretical and Applied Physics

Department of Theoretical and Applied Physics

African University of Science and Technology [AUST], Km 10 Airport Road, F.C.T Abuja, Nigeria

8/11/2023

DECLARATION

I, the undersigned, hereby declare that the work contained in this thesis is my original work, and that any work done by others or by myself previously has been acknowledged and referenced accordingly

ABSTRACT

Achieving efficient control of electrons and nuclei in atoms and molecules with lasers has been a subject of great interest for decades, in Physics and in Chemistry. One of the current and challenging questions with the today advanced in laser technology is how to generate and characterize a single and or a train of attosecond ($1\,as = 10^{-18}\,s$) laser pulses likely to control electrons in molecules. This therefore demands a proper mechanism that can lead to easy control of the extreme ultraviolet (XUV) harmonics.

This is addressed in this work by first irradiating the Hydrogen atom H with a single infrared (IR) pulse and later with simultaneous interaction with double replica IR lasers of intensity $2 \times 10^{14}\mathrm{W/cm^2}$ each. The order of frequency of emitted photons in the recombination process for two IR Lasers and for a single IR laser, interacting with the hydrogen atom without time delay, were 400 and 278, respectively. This High Harmonic Generation (HHG) of XUV's depends on laser atom interaction which is governed by Time Dependent Schrödinger Equation (TDSE) and the Strong Field Approximations (SFA). By varying the time delay between the two simultaneous IR pulses, controlled harmonics are produced. It turns out that these delays caused spectral shifts which are smaller for longer time delays (the spectral shift for 400 a.u. time delay is smaller than that of 1250a.u. time delay).

Keywords: Attosecond Pulse, Extreme ultraviolet pulses (XUVs), High-order Harmonic Generation (HHG), Split Operator Method, Three Step Model, Strong Field Approximation (SFA), Time Delay.

ACKNOWLEDGEMENT

During my research, I got the guidance and great supervision of Prof. Anatole Kenfack, who ensured that I did and completed my research successfully. My special appreciation goes to him and the entire department under his leadership as the H.O.D. It has been my pleasure to study in African University and Technology (AUST) under the AfDB scholarship.

My thanks and acknowledgement also go to my lecturers who ensured that I was well equipped and ready for my research through various class lectures and projects.

I also give to my classmates a warm appreciation for all discussions during my entire stay at AUST. Above all, the almighty God for the good health and the peace granted to me throughout.

In another special way, my appreciation goes to my family for their encouragement, their patience and their financial support.

Thank you all for contributing to the success of this research.

DEDICATION

I dedicate this work to my entire family who has always believed in me. I always appreciate your love and your care.

Table of Contents

List of Tables

Table of Figures

Chapter1 Introduction

1.1 Problem Statement

The growing applications of lasers in various fields such as photoemission spectroscopy has prompted the advancement of attosecond science. This development has enabled the study of fast occurring processes on electron level. To properly utilize and comprehend attosecond science, controlled attosecond pulses in form of Extreme Ultraviolet (XUV) harmonics should be produced. Therefore, this thesis aims at providing a proper mechanism of controlling XUV harmonics using double Infrared (IR) laser pulses.

1.2 Preliminary

Understanding some natural and human phenomena in life mostly depends on suitability of spatial and temporal scales used. In terms of better incorporation of spatial scales, a lot of geo-statistics analysis has been done [1]. But to date a lot more focus has been directed to the temporal scale. This opens the exploration of ultrashort pulses and now extreme ultraviolet (XUV) harmonics which is as a result of High-order Harmonic Generation (HHG) process in gases with high photon flux [2]. These XUV beams exhibit good spatial coherence and therefore HHG is a table top process to be considered [3] as it appears now as more complex than previously considered. Dedicated experiments and simulations are developed to understand and to control the harmonic beam spatial properties which is now the main arena for attosecond science [3]. The more we control XUV harmonics, the more applications in the field of medicine, photoelectron spectroscopy [4], time- and angle-resolved photoemission spectroscopy [5] and high-resolution transient absorption spectroscopy [6] are possible. The temporal and spatial scales of some physical phenomena include, the orbital period of the earth around the sun which is one year, the orbital period of the moon around the earth which is a month and the period of the heart palpitations which is a second (1s). These are considered within the human time scale and can be studied with available technologies. More fast occurring processes and activities like chemical reactions require sophisticated instruments with higher order processing times of zeptoseconds ($\sim 10^{-21}\ s$), attoseconds ($\sim 10^{-18}\ s$),

femtoseconds ($\sim 10^{-15}\ s$) to a few thousand femtoseconds or picoseconds ($\sim 10^{-12}\ s$) [7]. The timescale measurement of these chemical and other fast occurring biological process, has been enabled by more research on generation and control of laser pulses [7]. The femtosecond and attosecond laser sources are considered to be the main tools for resolving the fast electron motion in matter down to sub-Ångstrom $\left(1\ \text{Å} = 10^{-10} m\right)$ resolution [2]. The electron transition between states is a fundamental process in laser matter interaction. Until recently, it was not possible to observe the motion of the electrons, because there were no high-resolving tools available. But, with the advent of the attosecond ($10^{-18}\ s$) pulses (ATP) a new time perspective is opened [9]. A lot of experiments have been able to characterize most of the aspects of both the generation and filtering the ATP through optical gating which can generate ultra-broadband attosecond pulses using multi-cycle pulses [10], or ionization gating which genarates isolated attosecond pulses (IAPs) by controlling the ionization process in 3 step model [10]. To generate IAPs, scientists explore various methods, for instance using a sub-two-cycle driving laser with a stable carrier envelope phase (SCEP), or a longer driving laser with different gating methods to control the radiation process of HHG. The first successful demonstration of isolated attosecond pulses was achieved in 2001, in a system that used a selection around the cut-off generated in HHG with a 7fs long driver pulse [11]. This thesis makes used of the double IR laser pulse (two femtosecond pulses) to generate a single or a train of ATP that are at the origin of many hot research topics currently discussed in this field. The availability of Schemes to control spectral harmonics by using the time delayed IR pulses, proposed and experimentally verified [12], is also very crucial for this work. This makes a lot more interesting area to explore.

The spectrum of differrent temporal scales of natural phenomena and technological development to XUV region can be clearly seen in **Fig 1:1**.

The femtosecond and attosecond pulses have become one of the main tools to study both the electronic and molecular dynamics as shown in **Fig 1:1**.

During any attosecond pulse generation and analysis, it is fundamentally important to get better understanding of characteristics of a laser. The next subsection is dedicated in briefly describing these basics of the laser.

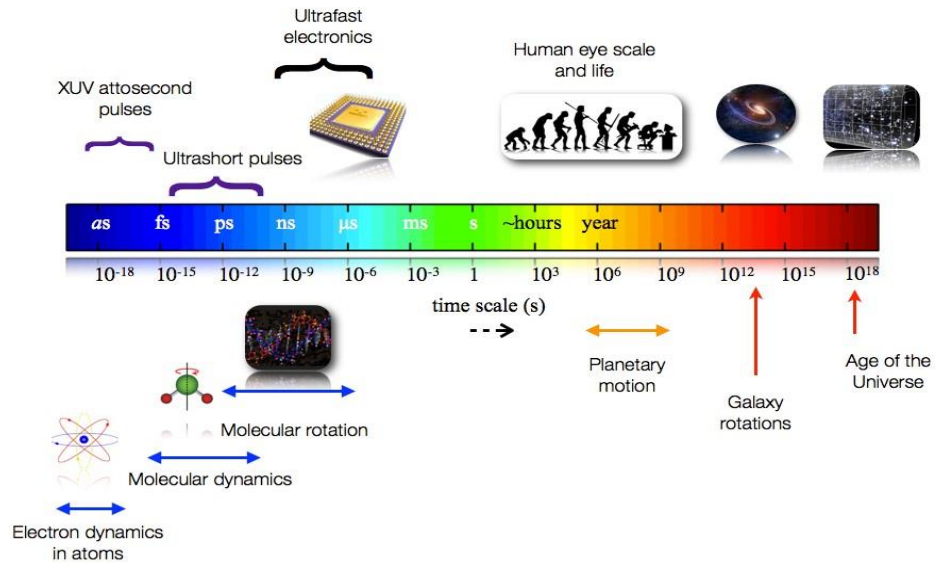

Fig 1:1 Timescale of differrent physical phenomena [8]

1.3 Laser Fundamentals

A laser which is an acronym for Light Amplification by Stimulated Emission by Radiation (LASER), is a device that emits light through a process of optical amplification based on the stimulated emission of electromagnetic (EM) radiation [36]. The first laser was built by Theodore H. Maiman based on a theoretical work by Charles Hard Townes and Arthur Leonard Schawlow in the year 1960 [15].

What makes a laser different from any other light is its high spatial and temporal coherence [16].

1.3.1 Components of a Typical Laser:

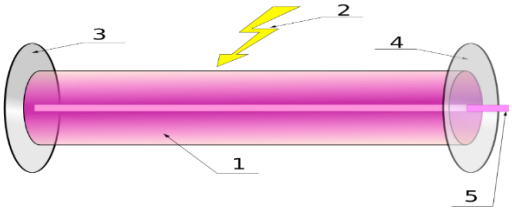

1. Gain medium
2. Laser pumping energy
3. High reflector
4. Output coupler
5. Laser beam

Fig 1:2 Components of Laser [58]

The gain medium is a material with properties that modulate the amplification of light via stimulated emission [18]. These properties are enhanced by the excitation system or a laser pump through a supply of necessary energy in the form of light or electric current. The active medium resonates between high reflector and partial reflector until there is a beam of single wavelength which is then released through the outer coupler as a coherent beam in the form of a laser [19]. The insights of a laser production are determined by the interaction of active medium with a photon from the pump medium. A number of processes are factored including the emission and absorption of photons, during which electron is caused to move to excited state or to the ground state, respectively, as it is illustrated in **Fig 1:3**. It is well known that an electron

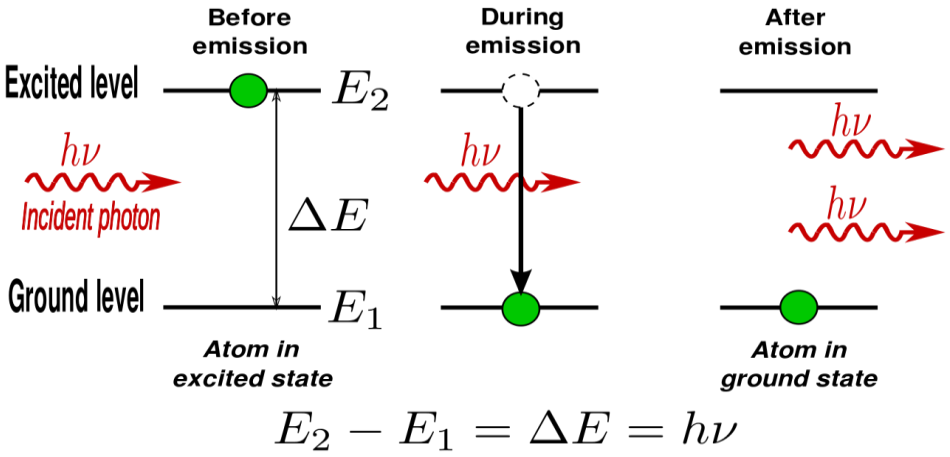

Fig 1:3 2-level Stimulated Emission [57]

absorbs a photon only when the transition energy matches the energy carried by the photon. For light, any given transition will only absorb light of particular wavelength. Photons with the energy that matches the energy difference between two energy levels can cause an electron to jump from the lower to the higher energy level through photon absorption process. This electron is thus in the excited state. When an electron is excited, it will not stay there forever; but it will eventually return to the ground state or to a stable state, leaving a vacuum with the energy matching ΔE. Due to the law of conservation of energy, spontaneous emission is likely to occur, where the electron transits to a lower or to an unoccupied energy level in the absence of any external [18]. The emitted photons from this process are in random directions, hence it is a suitable mechanism for fluorescence and thermal emission [21].

When a photon interacts with electrons in the excited state, stimulated emission occurs causing the electrons to drop from the higher to the lower energy level, emitting a new photon. These emitted photons are in phase, moving in the same direction and have the same wavelength.

At thermal equilibrium, the electron populations between any two-level system are given by a Boltzmann relation principle, also refer to as a fundamental law of thermodynamics [18];

$$N_2 = N_1 e^{\left(\frac{E1 - E2}{kT}\right)} \quad 1.1$$

Where N_2 and N_1 are the population of the upper and lower state, respectively. Here, E_2 and E_1 are energies corresponding to the upper and lower states, respectively, T represents the equilibrium temperature, k is the Boltzmann constant, and h is the Planck's constant whereas *v* represents the frequency of light. For a normal population of the atoms, there will always be more atoms in the lower energy state than in the upper ones [36]. In order to achieve stability after excitation, the electrons in the excited state will decay to ground state. When such a decay occurs due to spontaneous rather than stimulated emission, the produced photons deviate from proper characteristics of a laser [57]. To ensure the production of photons with laser characteristics, first, a relatively high number of atoms must be in the higher energy state than the lower energy state; this is done through a process commonly known as population inversion [57]. Besides, the natural decay of electrons to a lower state can avoided by introducing a photon to interact with the excited electrons, thereby causing instead a stimulated decay of electrons [36]. This is clearly shown in **Fig 1:3**. However, stimulated decay cannot be achieved with impractical 2-level system due to short lifespan of electron in excited state. Hence the need for a proper population inversion process in the subsequent higher-level systems [18].

Population Inversion

Population inversion is the process of achieving higher number of electrons in the higher energy states than the lower energy states. This is mainly used for light amplification and in production of a laser [57]. As stated previously, this process is not possible for 2-level system [42]. Therefore, three or more energy states are required to achieve a proper population inversion. The greater the number of energy state, the greater the optical gain [18].

3-level Laser

Considering a three energy levels system with E_1, E_2 and E_3 representing energy level one, two and three respectively, it is well known that $E_1 < E_2 < E_3$.

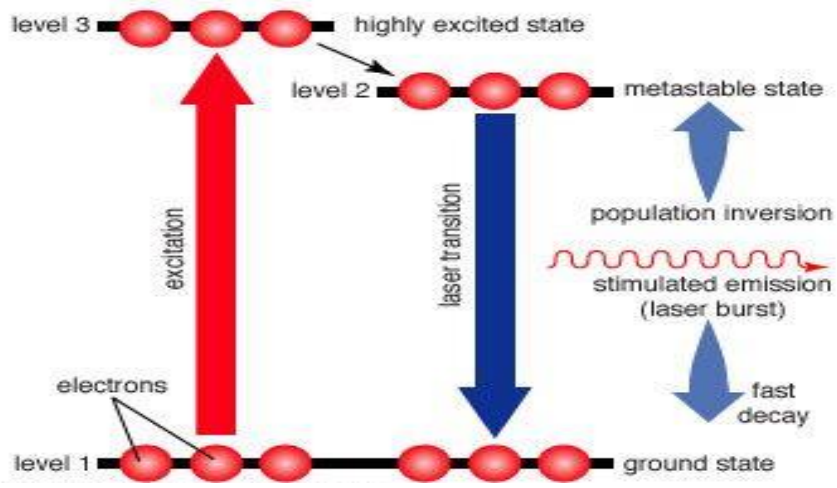

Fig 1:4 3 level system [58]

Letting N_1, N_2 and N_3 be the number of electrons in the energy state E_1, E_2 and E_3, respectively, in an equilibrium or in a stable system, with $N_1 > N_2 > N_3$. With a pumping process, the population inversion can be achieved between E_1 and E_2, such that $N_2 > N_1$ [18]. Upon excitation, the electrons jump to E_3 where their lifetime is very small and hence instantly falling to stable state [36]. Here, E_2 is a meta stable where the electrons will remain for some times during which $N_1 < N_2$ and $N_2 > N_3$. Here the population inversion is achieved between E_1 and E_2 [36].

After completion of lifetime of electrons in the Meta stable state, they fall back to the lower energy state by releasing energy in the form of photons and as a result, stimulated emission occurs [36]. In addition, the excitation of the electrons in this system may be through hitting with a photon or using other types of energy sources such as electrical energy. However, this requires very high pump power and produces pulsed laser [22].

4-level Laser

As shown in ***Fig 1:5***, a similar process to that of three-level system occurs with the meta stable state being E_3 [58]. Here we consider $E_1 < E_2 < E_3 < E_4$, where E_1, E_2, E_3 and E_4 represent energy level one, two, three and four, respectively.

When the electrons in the lower state E_1 gains sufficient energy and jumps into the higher energy state E_4 where lifetime of electrons is very small, they fall back into the next lower energy state E_3 by releasing non-radiation energy [58].

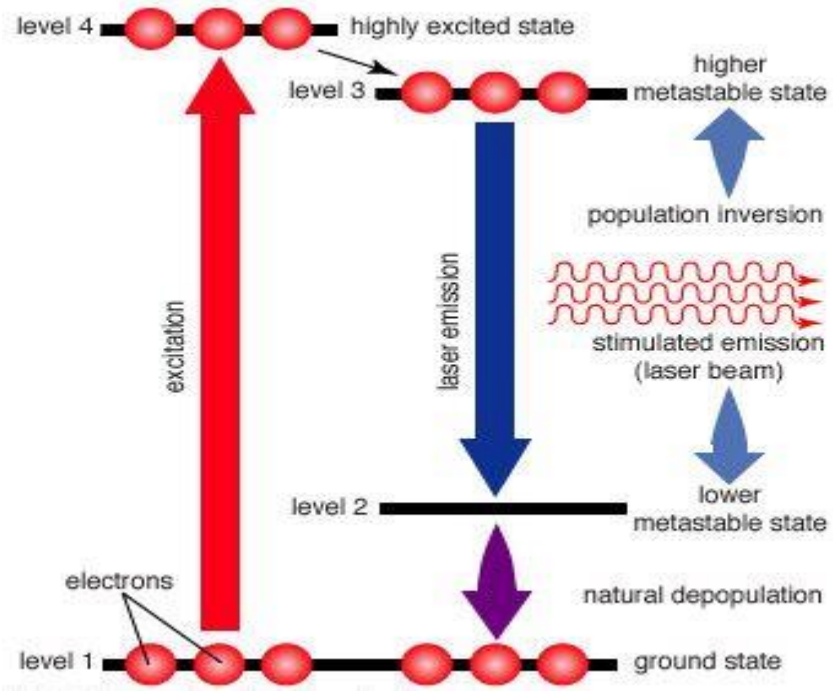

Fig 1:5 4-level system [58]

The lifetime of electrons E_3 is larger than that of E_4 and E_2. As a result, a large number of electrons accumulate in E_3 and hence a population inversion between energy states E_3 and E_2 is achieved [57].

This type of scheme can operate in continuous wave mode and hence used in most working lasers. It is a system which is also much easier to pump compared to 3-level scheme [36].

The kind of lasers generated are broadly categorized in two deterministic forms, depending on the output. The subsequent section is solely dedicated in describing the two forms, though the nature of our research adopts only one.

1.4 Continuous and Pulsed Wave Lasers

The classification of the two lasers depends on the output produce and the energy propagation. Pulsed laser produces a series of pulses at a certain pulse width and frequency until stopped

while continuous laser emits steady beam of light with constant power. Relaxation time is also fundamental in differentiating the two [18].

1.4.1 Continuous Wave Lasers (CW)

These are lasers whose outputs are steady over time, i.e., their output power is steady when averaged over any time period [57]. They have time durations in few nanoseconds or less. For a continuous laser operation, population inversion of the gain medium must have a steady pumping source, in order to ensure a steady streaming of wave. During steady pumping process, caution must be taken to prevent destruction of active medium by the excessive heat generated. Examples include Argon and CO_2 lasers [18]. The energy propagation for this type of laser is given by;

$$E(t) = E_0 \sin(\omega t + \varphi), \tag{1.2}$$

where E_0 is the amplitude of the laser, ω is the frequency and φ is the phase.

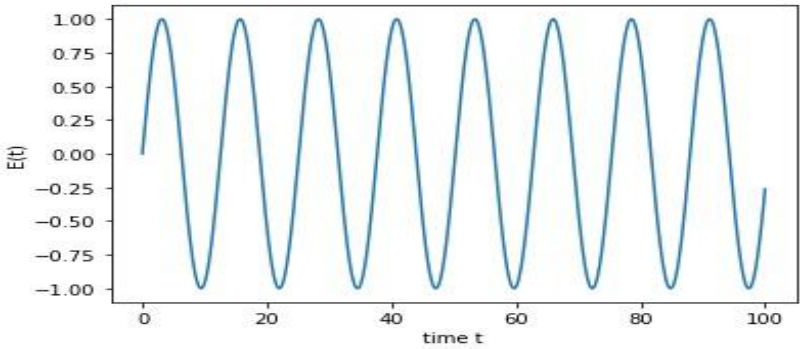

Fig 1:6 Continuous Laser [57]

1.4.2 Pulsed Lasers

These are lasers whose output occur as short bursts. This implies that the optical power of a pulsed laser appears in flashes/pulses of some duration at some repetition rate [57]. The average power P_{avg} is expressed as the average energy E of the laser divided by their repetition rate T ($P_{avg} = \frac{E}{T}$). By lowering the repetition rate, one can build more energy within a pulse. Pulsed lasers are particularly useful in applications where large amount of energy is required to be delivered in a short time. For this, researchers use more pulsed lasers because all the power of a laser appears to be concentrated within a pulse [57]. As mentioned before this will be the

form of the laser utilized in this thesis. ***Fig 1:7*** shows a pulse laser of 3 cycles in each of the five pulses. The energy propagation of this type of laser is given by:

$$E(t) = E_0 f(t) sin(\omega t + \varphi), \quad 1.3$$

where E_0 is the amplitude of the laser, ω is the frequency, φ is the phase, *f(t)* is the envelope, $f(t) = sin^2\left(\frac{\pi}{\tau_p}\right) t$ and τ_p is the pulse width.

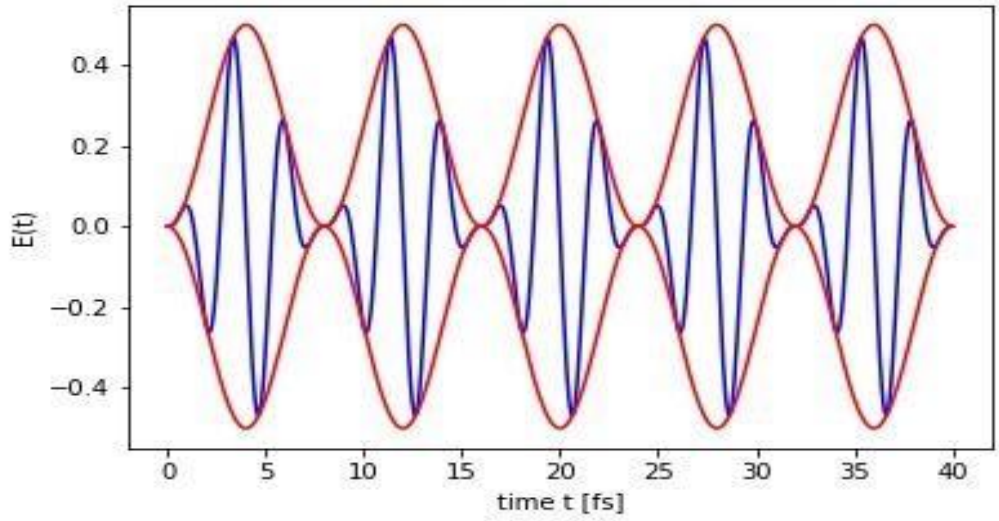

Fig 1:7 A Pulsed Laser [57]

1.5 Characteristics of a Laser

There are some specific properties that make a laser suitable to its application in production of XUV pulses. Studying these properties is the key to being intuitively able to have more control of transient pulses. Some of these characteristics are briefly described below [23].

Monochromaticity of Laser: The energy of a photon determines its wavelength through the relationship $E = hc/\lambda$, where c is the speed of light, h is the Planck's constant, and λ is the wavelength. In an ideal case, the laser emits photons with the same energy, and thus the same wavelength which makes it monochromatic. The light from a laser typically comes from one atomic transition with a single precise wavelength. Therefore, the laser light has a single spectral color and is almost the purest monochromatic light available [36, 57].

Types of Lasers and their wavelengths

The below table depicts some of the common laser based on wavelengths range.

Laser Type	Wavelength (nm)
Free electron	UV-Xray
Excimer: Argon fluoride	193
Nitrogen	337
Argon ion (blue)	488
Argon ion (green)	514
Helium Neon (blue)	633
Ruby (CrAlO3)	694
Rhodamine 6G Dye (tunnable)	570 – 650
Ti-Sapphire	**650 – 1100**
Nd: YAG	1064
Carbon dioxide	1064

Table 1:1 laser types [57]

Coherence: Light waves emitted by a laser are always in phase with each other at every point in the space, i.e., temporal and spatial coherence. Hence, a laser light beam is known as a coherent beam of light [57]. If coherent waves combine, then the amplitude of the resultant wave is always greater than the amplitude of any of the combining waves.

A wave is said to have a temporal coherence if the phase difference between the electric fields at a point in times t_1 and t_2 is constant during the time interval, Δt ($\Delta t = t_1 - t_2$).

Spatial coherence refers to the phase relationship between waves travelling side by side at a certain distance from each other [36, 57].

Directionality: This a property that makes a laser to travel in one direction only (without separating). This is also well known as collimation property of laser. The negligible divergence of the laser beam makes the laser useful in range finders, remote sensing, surveying [23] etc.

Intensity of Laser Light: The intensity I of a wave is defines as the energy per unit time per unit area**;** $I = \frac{E/t}{A} = P/A$ $(watt/m2)$.

Since a laser gives out the light into a narrow beam and the light energy is concentrated in a region of a small area, therefore, the intensity of the laser beam is very high [23].

For instance, the intensity of a 1mW laser is far much more, about a thousand times more, the intensity of a 100W incandescent bulb (ordinary electric bulb) [23]. A typical laser has the intensity of the order of $10^{13} Wcm^{-2}$, making them suitable for application such as cutting and welding metals and alloys [23, 25].

To produce XUV pulses, an IR laser in the form of Femtosecond Pulse (FP) is used and through HHG process, an attosecond pulse (ATP) is produced. In this work the second FP was introduced as a control mechanism.

Ultrashort Pulse Laser

This is a laser that generally emits pulses of femtosecond order and is also known as ultrafast laser. And owing to this, the current field of attosecond science has been inspired by the availability of common ultrashort pulse laser technologies such as Titanium-Saphire [9].

Since its implementation in 1960, a lot of techniques were employed to shape up to the current attosecond field [25]. Some of these are mentioned briefly as below.

The Q-Switching

This an active technique that modulates the losses in the cavity [26]. This technique is used to generate nanosecond pulses of high energy in solid-state lasers [27].

Kerr Lens Mode-locking (KLM)

It is a passive technique that uses the nonlinear Kerr effect to mode-lock lasers leading to very short emissions [28]. Depending on the synchronization spectrum phases, this method yields very short pulses of a few femtoseconds.

The evolution of ultrafast pulses from basically its first implantation to current attosecond science, can be briefly shown in the **Fig 1:8** *Timescale of evolution of ultrafast Pulses [28]*.

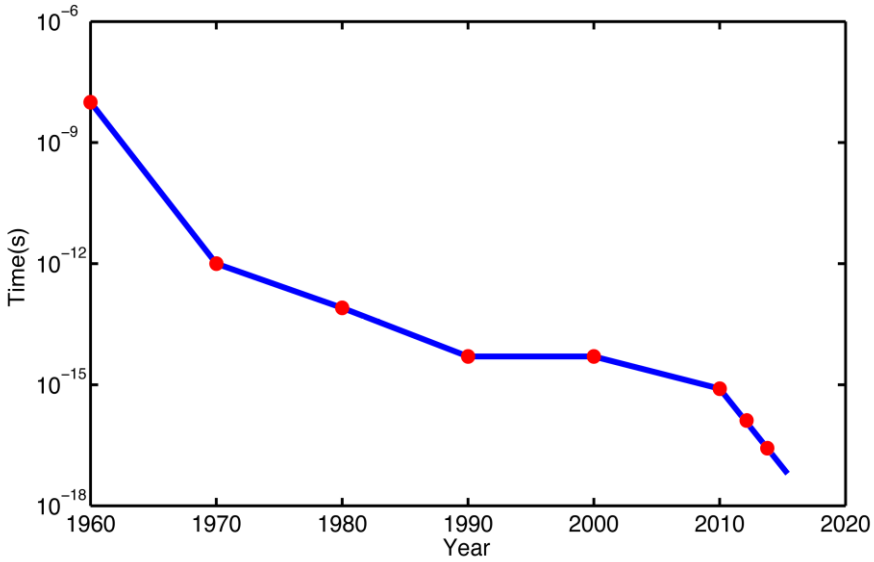

Fig 1:8 Timescale of evolution of ultrafast Pulses [28]

To get the insights of an attosecond pulse generation the amazing phenomena of HHG process must be studied in detailed [29]. The next section is dedicated to discussing laser-matter interaction and the HHG process.

Chapter2 High-order Harmonic Generation

In this part, we are going to explore the theoretical aspects of High-order Harmonic Generation (HHG). HHG is a nonlinear optical process in which the frequency of laser light is converted into its integer multiples [19]. Harmonics of very high orders are generated from atoms and molecules exposed to intense (usually near-infrared (IR)) laser fields [7].

The first HHG was observed in 1977 in interaction of intense CO_2 laser pulses with plasma generated from solid targets, by scientists who were interested in the response of atoms to intense laser fields [13]. When the atom is exposed to such intense laser field, an electron detaches through ionization and move to the continuum before recombining with its parent atom. The electron motion in the continuum can take long or short trajectories [14],

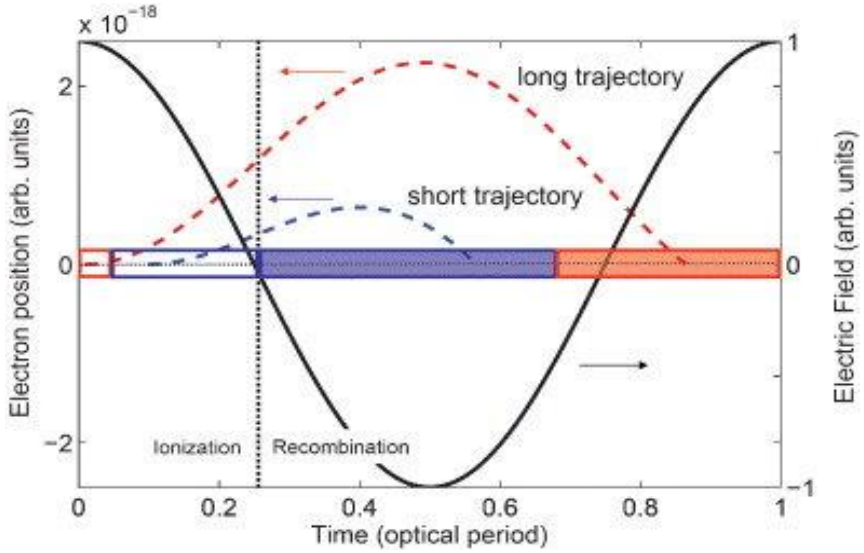

Fig 2:1 Concept of Two electron trajectories in a Driving Laser field [14].

depending on oscillating electric field as shown in **Fig 2:1**. Upon re-collision, photons of high harmonics are emitted [57]. The first results of HHG obtained by Rhodes and his co-workers, using a 248-nm excimer laser, were up to 17^{th} harmonic order [30]. The motion of electron from the time of excursion to recombination can be described using classical and quantum schemes [57].

2.1 Electron Dynamics in the Continuum

Taking the classical approach, the electron in a polarized laser field is described by Newton laws of motion [57].

The polarized electric field is described by the equation below.

$$\vec{E} = E_0\, cos(\omega t + \varphi)\, \vec{e}_z \tag{2.1}$$

Where $\vec{e}_z$ is the unit vector along the z-axis, ω the frequency, φ the phase shift and E_0 the amplitude with the Hamiltonian of free electron given as;

$$H(t) = \frac{p^2 y}{2m} + qyE_0\, cos(\omega t + \varphi) \tag{2.2}$$

Where $q(electric\ charge) = e, p_y(linear\ momentum) = m\frac{dy}{dt}$ and $e = m = 1a.u.$ in atomic units.

With the Newton equations $\frac{dy}{dt} = \frac{dy}{dp_y}$, $\frac{dp_y}{dt} = -\frac{dH}{dy}$ and $\frac{dp_y}{dt} = -q\, E_0 cos(\omega t + \varphi)$ the resulting equation is an Ordinary Differential Equation (ODE)

$$\frac{d^2 y}{dt^2} = -E_0\, cos(\omega t + \varphi) \tag{2.3}$$

Whose integration yields,

$$\frac{dy}{dt} = -\frac{E_0}{\omega} sin(\omega t + \varphi) + constant \tag{2.4}$$

Applying the initial conditions to the above equation

$constant = \left(\frac{\mathrm{dy}}{\mathrm{dt}}\right)(t = 0) + \frac{E_0}{\omega} sin(\varphi)$,

This constant stands for the drift velocity v_D. With $y(t = 0) = y_0$, the position of electron can be deduced from the velocity equation eq.2.4 above as:

$$y(t) = v_D t + \frac{E_0^2}{\omega^2} cos(\omega t + \varphi) + y_0 \quad 2.5$$

This shows that as the electron oscillates with the electric field and is being drifted with velocity v_D
From eq.2.4 it is clear that the velocity of the electron oscillates with frequency ω and amplitude $\frac{E_0}{\omega}$ around the drift velocity v_D.

The kinetic energy of the drifting electron in polarized laser field can be evaluated as;

$$E_{kin} = \frac{1}{2}\left(\frac{dy}{dt}\right)^2 = \left(v_D - \frac{E_0}{\omega} sin(\omega t + \varphi)\right)^2 \quad 2.6$$

Over an optical cycle with pulse period T, the average kinetic energy will be stated as;

$$\langle E_{kin} \rangle = \frac{1}{T} \int_0^T dt \left(\frac{1}{2} v_D^2 + \frac{E_0^2}{2\omega^2} sin^2(\omega t + \varphi) - \frac{E_0}{\omega} v_D \, sin(\omega t + \varphi)\right) \quad 2.7$$

And by integration, it reads

$$\langle E_{kin} \rangle = \frac{1}{2} v_D^2 + \frac{E_0^2}{4\omega^2} \quad 2.8$$

Where $\frac{E_0^2}{4\omega^2} = U_p$ is the ponderomotive energy that arise due to quiver motion of electron in the laser field [57].

During the recombination process, the HHG spectra exhibits characteristic behaviour. The produced photons have a rapid intensity decrease for the first orders, a plateau harmonic up to a very high order and an abrupt cut-off [57], as seen in **Fig 2:2**

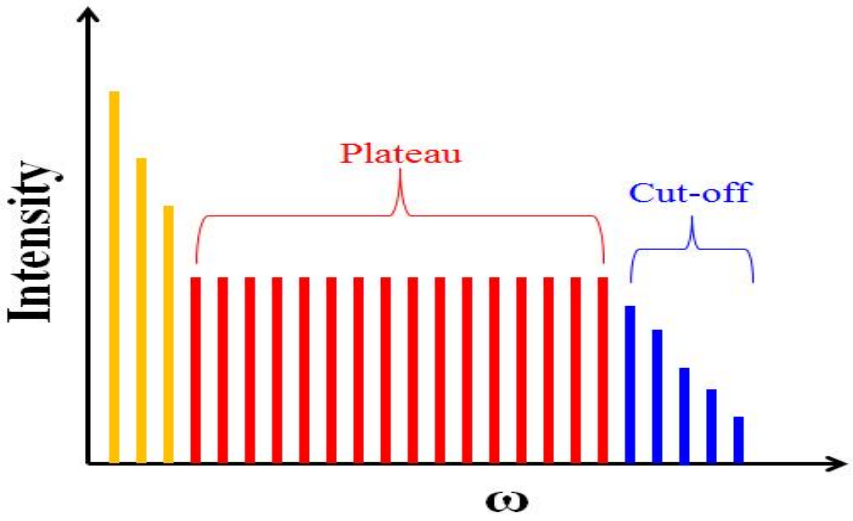

Fig 2:2 Schematic Representation of the HHG Spectrum [30].

Due to its coherence, HHG is a process that plays a fundamental role in the generation of pulses in XUV and in soft X-rays range [31].

The maximal harmonic photon energy E is given by the cut-off law [57].

$$E = I_p + 3.17U_p \tag{2.9}$$

Where I_p is the ionization potential of the target atom.

Rather than using the perturbation theory, many features of HHG can be intuitively and quantitatively explained in terms of electron re-scattering trajectories. This represents the semiclassical three-step model and the quantum-mechanical Lewenstein model. Remarkably, various predictions of the three-step model are elaborated by a direct solution of the time-dependent Schrodinger equation (TDSE) [35].

2.2 Three Step Model

The underlying process of HHG is well elaborated by the Three Step Model as used in the previous subsection [32]. This model consists of tunneling where the electron is treated quantum mechanically as it ionizes. This is well described in the subsection above. It also consists of acceleration and recombination process during which the electron is treated classically [57]. This is a semiclassical model used to verify some of the results obtained from experiments and therefore it will be explored later in chapter 5 to verify results of this thesis.

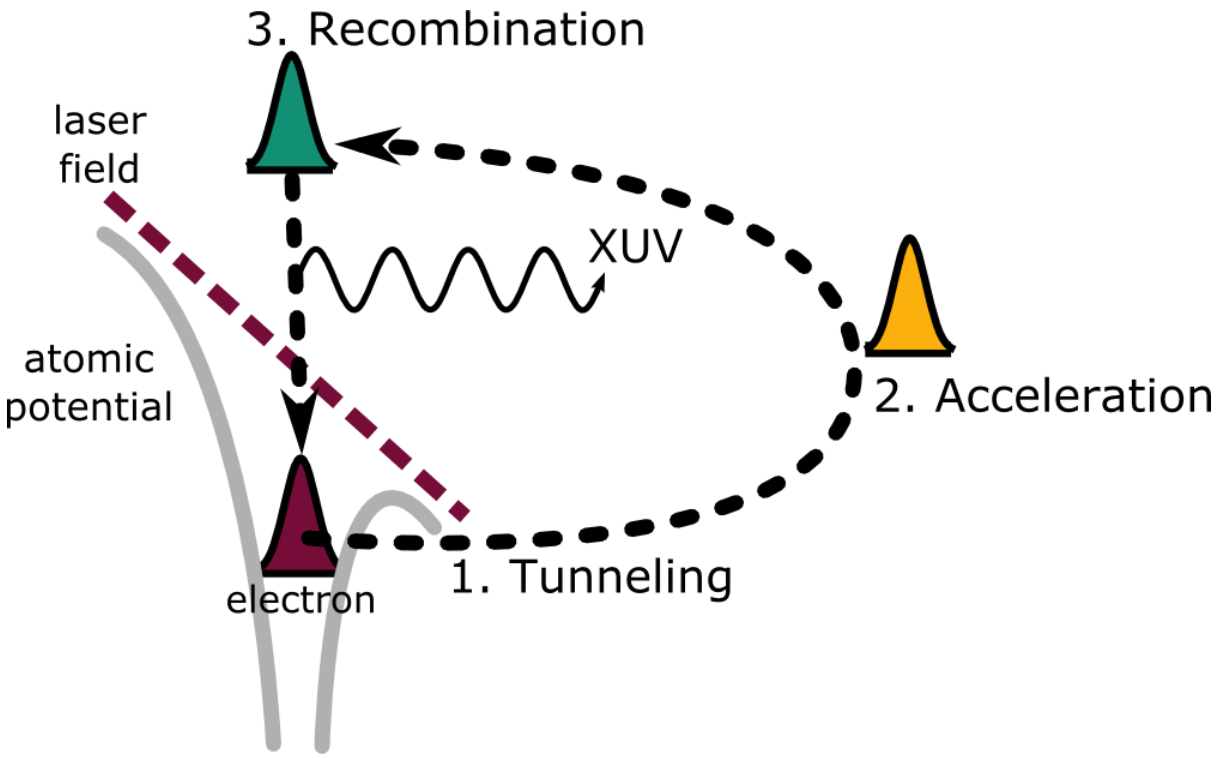

Fig 2:3 Classical Scheme of HHG process [57]

2.2.1 Tunneling

When an atom is placed in the path of a laser field, it is ionized thereby forcing excursion of electron. To achieve this ionization the supplied energy should be greater than ionization energy I_p. A single photon produces an energy of $\hbar\omega = \omega$ and $\omega < I_p$. This implies a single photon is not enough hence the need of multiphoton ionization with energy of nω order [57], where n is the number of photons. Tunneling occurs when the Keldysh parameter $\gamma < 1$, with $\gamma = \sqrt{I_p / 2U_p}$, implying that $U_p \geq I_p$. The barrier is suppressed by strong laser field $(\omega \ll I_p)$ and hence electron tunnels through.

$$\omega(E) \approx exp\left(-\frac{2(2I_p)^{3/2}}{3E}\right) \qquad 2.10$$

Where $\omega(E)$, is the ionization rate.

The probability of finding the atom in the ground state can be stated as;

$$|a(t)|^2 = exp\left(-\int_{t_0}^{t} \omega(E(t'))\, dt'\right) \quad 2.11$$

a(t) is the probability amplitude of finding the atom in the ground state and t_0 is the time for which the electron is released by the atom [56].

2.2.2 Acceleration

After ionization, the electron is then propagated in the continuum, during which there is acceleration of electron in the presence of electric field induced by the laser [57]. Assuming that electron is released with zero velocity, then the acceleration will be given by eq.2.3. From eq.2.5 we derive the trajectories in **Fig 2:1**

According to 3-step Model, HHG is due to the emission on re-collision. This therefore makes the kinetic energy of the electron fundamental. This kinetic energy is proportional to $3.17U_p$ as indicated by eq.2.8 [17].

2.2.3 Recombination

This step describes the re-collision process of the electron with an atom. Since we are describing the electron from excursion to re-collision, this is a quantum mechanical process and is described by the Time Dependent Schrödinger Equation (TDSE). Taking into account Strong Field Approximation (SFA), the equation describing this process is given as;

$$i\frac{d}{dt}\psi(t) = H\psi(t) - xE(t), \quad 2.12$$

with the atomic Hamiltonian given by

$$H = -\frac{1}{2}\nabla + V(x), \quad 2.13$$

where $V(x)$ is the effective atomic potential confining the electron to the atom. Due to the interaction with the laser field, it is expected that the wavefunction of the electron that is initially in the ground state $|0\rangle$ evolves into a superposition state between the ground state with

probability amplitude *a(t)* and a wavefunction describing free electron or the continuum state, $|\psi_c(t)\rangle$.

$$|\psi(t)\rangle = a(t)|0\rangle + |\psi_c(t)\rangle \qquad 2.14$$

Though the free electron together with the parent atom form a dipole moment, this is not the source of emitted EM radiation. Dipole acceleration is rather the contributing source of HHG [35]. This acceleration of the electron dynamics of this process is revealed numerically by direct integration of the TDSE. A simple example of the harmonic field made up of the of odd harmonics is shown in **Fig 2:4**

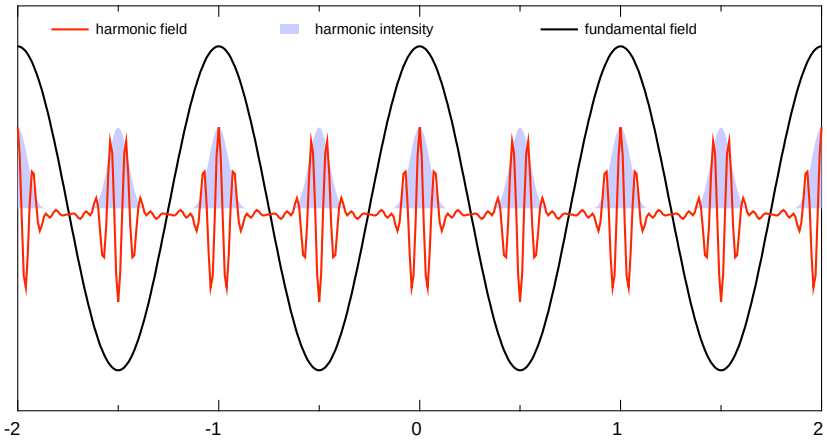

Fig 2:4 Train of Attosecond Pulses [33].

This kind of pulse could experimentally be obtained through the following set up of HHG in **Fig 2:5**

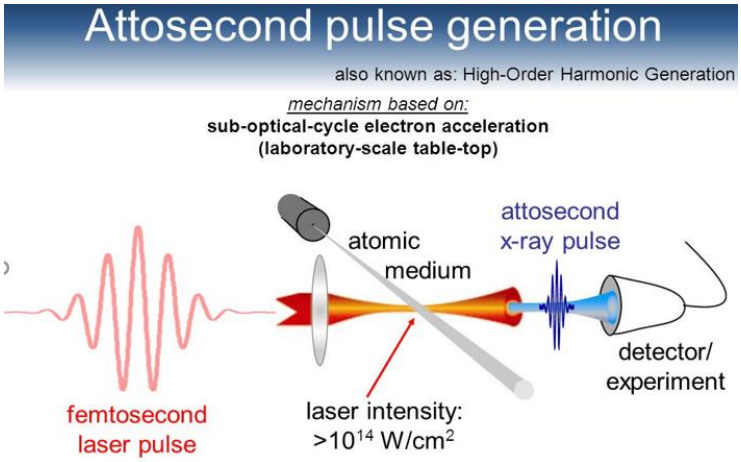

Fig 2:5 Experimental set up of Attosecond Pulses [18]

2.3 Lewenstein Model

It is the analytical quantum theory of HHG developed by Lewenstein [34]. The analytical analysis of this model is based on the SFA assumptions [59]. These assumptions include neglecting the contribution of all the excited bound states, the effect of the atomic potential on the motion of electron in the continuum and the depletion of the ground state [59].

The majority of strong field effects can be understood at least qualitatively by this model which has less computational demand than numerically solving TDSE [59]. Using these SFA, the time-dependent wave function of Schrödinger equation can be expressed in the terms of ground state and continuum state [60], by considering an atom in SFA approximation in an intense field $E(t)$. This interaction of an atom with the intense field, linearly polarized in the x direction, can be described by TDSE in the length gauge,

$$i\frac{\partial\psi(x,t)}{\partial t} = (H(t) + xE(t))\psi\,(x,t), \tag{2.15}$$

where the Hamiltonian H is given as:

$$H(t) = H_0 + x.E(t) \tag{2.16}$$

And H_0 can be represented as the equation below

$$H_0 = -\frac{1}{2}\frac{\partial^2}{\partial \mathrm{x}^2} + \mathrm{V(x)}, \tag{2.17}$$

where $V(x)$ denotes the atomic potential. Therefore eq.2.17 determines the ground state of the system as;

$$H_0|g\rangle = -I_p|g\rangle \tag{2.18}$$

In the continuum electron is described as

$$H_0|k\rangle = \frac{k^2}{2}|k\rangle \tag{2.19}$$

Where k is the momentum of outgoing electron.

After transforming to the laboratory frame [60, 61], the induced dipole moment becomes,

$$D_x(t) = i\int_0^{\infty} d\tau \left(\frac{\pi}{\varepsilon + \frac{i\tau}{2}}\right)^{\frac{3}{2}} \left[cos\theta\ d_z^*(t) + sin\theta\ d_y^*(t)\right] \times \left[cos\theta\ d_z(t-\tau) + sin\theta d_z(t-\tau)\right]E(t-\tau) \times \exp[-iS_{at}(t,\tau)]\, a^*(t)a(t-\tau) + c.c, \quad 2.20$$

where ε is small positive constant; $a(t)$ is the amplitude of the ground sate; $d(t) \equiv d[P_{st}(t,\tau) + A(t)]$, $d(t-\tau) \equiv d[P_{st}(t,\tau) + A(t-\tau)]$ are transition-dipole moment between the ground and the continuum state, with P and A are canonical momentum and vector potential of the laser field respectively [60]; $P_{st}(t-\tau) = \int_{t-\tau}^{t} A\mathrm{t}'dt'/\tau$ is the momentum at the stationary point of the action.

The quasi-classical action at the stationery point is

$$S_{st}(t-\tau) = \int_{t-\tau}^{t} \left(\frac{[P_{st}(t-\tau) - A(\mathrm{t}')]^2}{2} + I_p\right) dt' \quad 2.21$$

Eq.2.20 and eq.2.21 are standard forms of equations in this model for the laser induced dipole moment [60]. Some of the SFA approximation will be extended in the next section of solving TDSE.

The importance of this model is that most of the simulations are done under the SFA and with slight improvement with the inclusion of field and atom interaction term, one can now obtained justifiable results from direct simulation of TDSE [20].

This model predicts the cut off energy E_c,

$$E_c = 3.17U_p + I_{p,} \quad 2.22$$

where $g \approx 1.3$. This prediction of the cut off energy is slightly higher than that of the 3-step Model [34].

Another model is the gaussian. This model is useful when one wants to account for the effect of the initial spatial width of the wave function within the framework of the Lewenstein model [35].

Atomic Units

Since all calculations in this thesis are in atomic units. **Table 2:1** Atomic Units [57] provides an overview of the units used in this work [57]

Quantity	Atomic units [au]	SI units [SI]
$\hbar$	1	$1.05457\times \mathbf{10^{-34}kg\ m^2/s}$
$\mathbf{m_e}$	1	$9.10939\times \mathbf{10^{-31}kg}$
E	1	$1.6028\times \mathbf{10^{-19}A.s}$
C	137.036	$2.99792\times \mathbf{10^{8}m/s}$
Time	1	$2.41888\times \mathbf{10^{-2}fs}$
Position	1	$5.29177\times \mathbf{10^{-2}nm}$ ($\mathbf{a_0}$: **1 Bohr**)
Velocity	1	$2.188\times \mathbf{10^{6}m/s}$
Electric field	1	$5.1427\times \mathbf{10^{9}/cm}$
Frequency	1	$4.1341\times \mathbf{10^{16}s^{-1}}$
Energy	1	$4.3597\times \mathbf{10^{-18}J}(\mathbf{Hatree, 2Ry}) = \mathbf{27.211}eV$
Permittivity	$1/4\boldsymbol{\pi}$	$8.8542\times \mathbf{10^{-12}As/Vm}$

Table 2:1 Atomic Units [57]

2.4 Theoretical Model

At the atomic time and space scales, the electron structure and electron dynamics description of the matter is fully governed by the laws of Quantum Mechanics. Typically, the study of the Quantum phenomena has been performed within the frame of the perturbative theory. It is a very good approximation in case that the coupling interaction potential of the system with an external field can be considered as a perturbation of the field-free Hamiltonian [21]. This theoretical approach has been quite successful to explain an ample range of experimental results [22, 24]. However, in case of ultrashort and ultra intense laser pulses, the interaction term can not be treated any more as a perturbation of the field-free Hamiltonian. A new and totally different theory needs to be developed in order to explain the experimental results in this regime. The most general treatment of the Quantum Mechanics is the Time Dependent Shrödinger Equation. It governs the time evolution of a wavefunction and with it, a quantification of the observables can be obtained.

In order to fully obtain the characteristics of the XUV lasers, we are going to exploit more on quantum approach by studying more on time dependent Schrödinger equation (TDSE). TDSE carries more information of how ultrashort laser (femtosecond wave) interact with atoms or

molecules. In this thesis we will use this approach to numerically analyze laser atom interacting.

This process is possible only if we solve TDSE equation [20, 37, 40]. The aim of this work is that we are going to consider a 1D TDSE in the form;

$$i\,\frac{\partial\psi(x,t)}{\partial t} = -\,\frac{1}{2}\frac{\partial^2}{\partial x^2}\psi(x,t) \;+\; V(x)\psi(x,t) \;+\; H_I\psi(x,t) \qquad 2.23$$

Where $\psi(x,t)$ is time-dependent wavefunction at position x at time t, $V(x)$ is the atomic binding potential, coulomb potential, $H_I = -xE(t)$ describes the atom-field interaction Hamiltonian within dipole approximation.

The next section provides a brief description of numerical algorithms used for solving the TDSE, where the time dependent quantum evolution of a wavefunction is used to compute the observables of interest. TDSE simulation is a powerful tool to investigate quantitative details, especially the effects of excited levels and the atomic Coulomb potential as well as gaussian potential [36].

Chapter3 Numerical Methods

Over time, many numerical methods used for solving the Time Dependent Schrödinger Equation (TDSE) have been developed. Some of these methods utilizes the Single Active Electron (SAE) approximations and are briefly discussed below.

3.1 Finite Difference Method

This is a method that converts the nonlinear partial differential equations (PDE) e.g., TDSE into a linear matrix equation. This is done by using finite difference approximations [37].

This procedure transforms the region (where the independent variables in PDE are defined on) to a mesh grid of points where the dependent variables are approximated [37, 38]. However, this method is too slow and computationally heavy for its use to be justifiable [38].

3.2 Pseudo-spectral Method

The fundamental concept of this method is to expand the solution function as a finite series of smooth basis functions [42]. For TDSE, the spatial parts of a wavefunction are discretized into grids by a synthetic scheme [40, 41].

Unlike Finite Difference Method, Pseudo-spectral Method is computationally less intense and it produces highly accurate and stable solutions [39]. However, this method has up to 20% error in the measurement of intensity [62].

3.3 Crank-Nicolson Method

This is a finite difference method developed by John Crank and Phyllis Nicolson in the mid 20th century [20]. It is a second order method in time that can be written as an implicit Runge-Kutta. Due to its numerical stability, it can be used for solving the heat equation as well as partial differential equations e.g., TDSE [43].

3.4 Split Operator Method

This method was developed by Feit and Fleck for solving TDSE [32]. It is one of the simplest and fastest methods for solving TDSE and it is widely used throughout modern quantum research, in particular when dealing with the Non-linear Schrödinger Equation (NLSE). it is the method used in this thesis and therefore its analytical derivation is shown below.

We considered a 1-D TDSE given by;

$$i\frac{d}{dt}|\psi(x,t)\rangle = \widehat{H}|\psi(x,t)\rangle \tag{3.1}$$

Where Ĥ is Hamiltonian. The solution of the above equation can be expressed as

$$|\psi(x,t+\Delta t)\rangle = U(t,t+\Delta t)|\psi(x,t)\rangle \tag{3.2}$$

Where $|\psi(x,t+\Delta t)\rangle$ is the evolved wavefunction, $|\psi(x,t)\rangle$ is the initial wavefunction, $U(t,t+\Delta t)$ is the Evolution Operator and Δt is the time interval or time step as referred to throughout this work.

We used the Split Operator Method to solve eq.3.1 by first splitting the Ĥ as the sum of two; the kinetic energy operator (T) and potential energy operator (V). These operators acts on momentum and position space, respectively [44].

Substituting the evolved wavefunction, $|\psi(x,t+\Delta t)\rangle$, in eq.3.2 into eq.3.1, the resulting equation is;

$$|\psi(x,t)\rangle i\hbar\frac{d}{dt}U = HU(t,t+\Delta t)|\psi(x,t)\rangle \tag{3.3}$$

This reduces to,

$$i\frac{d}{dt}U = HU(t,t+\Delta t) \tag{3.4}$$

which is a first order differential equation that can be solved as eq.3.5.

$$\int \left(\frac{dU}{U}\right) = -i\hat{\mathrm{H}} \int_{t}^{t+\Delta t} dt \tag{3.5}$$

Since Δt is so small, the above integration solves to,

$$lnU = -i\hat{\mathrm{H}}t \tag{3.6}$$

Thus, giving the evolution operator in terms of $\hat{\mathrm{H}}$ as;

$$U(t, t+\Delta t) = e^{-i\hat{\mathrm{H}}\Delta t} \tag{3.7}$$

With this form of evolution operator, the evolved wavefunction in eq.3.2 now reads;

$$|\psi(x, t+\Delta t)\rangle = e^{-i\hat{\mathrm{H}}\Delta t}|\psi(x, t)\rangle \tag{3.8}$$

But $\hat{\mathrm{H}} = T + V$. Therefore, eq.3.8 now reads;

$$|\psi(x, t+\Delta t)\rangle = e^{-i(T+V)\Delta t}|\psi(x, t)\rangle \tag{3.9}$$

Since T and V are noncommutative, we used Baker-Campbell-Hausdorff approximation formula stated by eq.3.10 below [57].

$$e^{(T+V)\Delta t} = e^{\alpha T} e^{\alpha V} e^{-\frac{\alpha^2}{2}[T,V]} e^{\frac{\alpha^3}{6}(2[V[T,V]]+[V[T,V]])} e^{-\frac{\alpha^4}{24}(\ldots[T,V]\ldots)} \tag{3.10}$$

If $\Delta t \to 0$ α goes to zero with the order $0(\Delta t^2)$ or higher, eq.3.10 reduces to eq.3.11 below.

$$e^{(T+V)\Delta t} = e^{\alpha T} e^{\alpha V} \tag{3.11}$$

By applying this approximation on eq.3.10 and substituting $\alpha = -i\Delta t$, we get either eq.3.12 or eq.3.13. These two equations represent two main schemes of Split Operator Method,

$$|\psi(x, t+\Delta t)\rangle = e^{-\frac{iV}{2}\Delta t} e^{-iT\Delta t} e^{-\frac{iV}{2}\Delta t}|\psi(x, t)\rangle \tag{3.12}$$

and

$$|\psi(x,t+\Delta t)\rangle = e^{-\frac{iT}{2}\Delta t} e^{-iV\Delta t}\, e^{-\frac{iT}{2}\Delta t} |\psi(x,t)\rangle \qquad 3.13$$

In this thesis we used the scheme governed by eq.3.12. This is because the last operation is in real space, hence requires a simple direct multiplication. Scheme governed by eq.3.13 requires an extra step, i.e., Inverse Forward Fourier Transform (IFFT), to take the wavefunction to the real space. By applying Forward Fourier Transform (FFT), wave-packet can be transformed from position to momentum space [44].

Considering first scheme, eq.3.12, we first performed half step in the position space by multiplying the wavefunction with exponential of potential V as shown by eq.3.14.

$$e^{-\frac{i}{2}V\Delta t}|\psi(x,t)\rangle = |\psi(x,t)\rangle' \qquad 3.14$$

Secondly, before performing the full step in momentum space, we transformed the wavefunction from position to momentum by taking the FFT of the position wavefunction, $|\psi(x,t)\rangle'$, from eq.3.14. The mathematical operation of this FFT is shown as; eq.3.15 results in a wavefunction is in momentum space.

$$|\psi(p,t)\rangle = \mathcal{F}\left(|\psi(x,t)\rangle'\right) = \frac{1}{2\pi}\int (dx)|\psi(x,t)\rangle' e^{-i\,px} \qquad 3.15$$

Where the resulting wavefunction, $|\psi(p,t)\rangle$, is in momentum space. Therefore, eq. 3.12 now reads;

$$|\psi(x,t+\Delta t)\rangle = e^{-\frac{i}{2}V\Delta t} e^{-iT\Delta t}|\psi(p,t)\rangle = e^{-\frac{i}{2}V\Delta t}|\psi(p,t)\rangle' \qquad 3.16$$

Where $|\psi(p,t)\rangle' = e^{-iT\Delta t}|\psi(p,t)\rangle$

Finally, before performing a half step in position space in eq.3.18, we took IFFT of the momentum wavefunction, $|\psi(p,t)\rangle'$, as shown by eq.3.17

$$|\psi(p,t)\rangle'' = \mathcal{F}^{-\prime}\left(|\psi(p,t)\rangle'\right) = \frac{1}{2\pi}\int (dx)\,|\psi(p,t)\rangle' e^{i\,px} \qquad 3.17$$

$$|\psi(x,t+\Delta t)\rangle = e^{-\frac{i}{2}V\Delta t}|\psi(x,t)\rangle'' \quad 3.18$$

The **Fig 3:1** below is a simple schematic representation of Split Operator Method used for solving eq3.12. This figure represents a process of propagating a wavefunction through real space in step one, momentum space in step two and real space in step three. It is important to note FFT and IFFT are required to be performed between step one and two and step two and three, respectively.

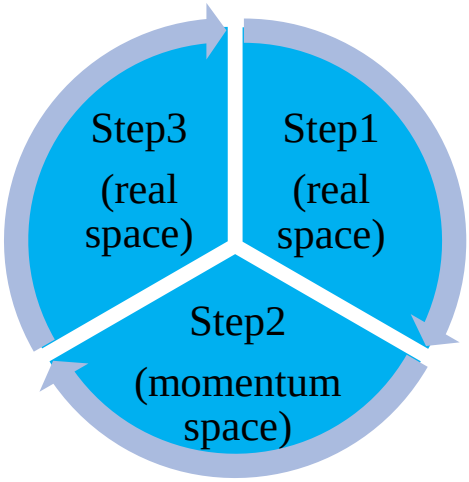

Fig 3:1 Schematic Representation of Split Operator Method

The wavefunction in eq.3.18 can be used in the computation of the average kinetic energy, $\langle E_{kin}\rangle$, and average potential energy, $\langle E_{pot}\rangle$, of the electron.

The kinetic energy T is given by:

$$E_{kin} = T = \frac{p^2}{2m} \quad 3.19$$

Thus,

$$\langle E_{kin}\rangle = \langle\psi(x,t)|T|\psi(x,t)\rangle$$
$$\langle E_{kin}\rangle = \left\langle\psi(x,t)\left|\frac{p^2}{2m}\right|\psi(x,t)\right\rangle \quad 3.20$$

Over pulse duration T_p, $\langle E_{kin}\rangle$ is given as;

$$\langle E_{kin}\rangle = \int_0^{T_p} \psi^*(x,t)\int\left(\frac{p^2}{2m}\right)dx\,\psi(x,t)\;dt \quad 3.21$$

And potential energy V given by;

$$E_{pot} = V = V_{soft\ core} - \int E(t)\, dx, \tag{3.22}$$

is made up of the soft-core potential $V_{soft\ core}$, where $V_{soft\ core} = -\frac{1}{\sqrt{x^2+a^2}}$ with a soft-core parameter a and electric field $E(t)$. This electric field takes the form given by eq.3.23 below.

$$E(t) = f(t)E_0 \cos(\omega t + \varphi) \tag{3.23}$$

Where, $f(t)$ is the envelope and E_0 is the amplitude of the Laser field.

With electric field from eq.3.23 , Potential energy in eq.3.22 becomes;

$$\mathrm{V} = V_{soft\ core} - f(t)E_0 \cos(\omega t + \varphi) \int dx \tag{3.24}$$

$$\mathrm{V} = V_{soft\ core} - xf(t)E_0 \cos(\omega t + \varphi)$$

Thus, average potential energy, $\langle E_{pot} \rangle$, is given by;

$$\langle E_{pot} \rangle = \langle \psi(x,t)|V|\psi(x,t)\rangle \tag{3.25}$$

Using eq3.24, this can be written as eq.3.26 below.

$$\langle E_{pot} \rangle = \left\langle \psi(x,t) \middle| \left(-\frac{1}{\sqrt{x^2+a^2}} - xE_{01}f(t)cos(\omega t + \varphi) \right) \middle| \psi(x,t) \right\rangle \tag{3.26}$$

Whose average over a pulse duration T_p is;

$$\langle E_{pot} \rangle = -\int_0^{T_p} \left(\psi^*(x,t) \int \left(\frac{1}{\sqrt{x^2+a^2}} + xE_{01}f(t)cos(\omega t + \varphi) \right) dx\, \psi(x,t) \right) dt \tag{3.27}$$

3.4.1 Dipole Acceleration of the Atom

The dipole acceleration is used to describe the ion-electron motion. This kind of acceleration is caused by the overlap of acceleration part of wavefunction and that in the core as well as the second derivative of the position of the electron density.

By Ehrenfest theorem [63],

$$m\frac{d}{dt}\langle x\rangle = \langle\frac{\partial x}{\partial t}\rangle_t + i\langle[H,x]\rangle \quad 3.28$$

where $[H,x] = Hx - xH$ is the commutator relation between H and x.

To calculate the dipole acceleration, we first start with the Hamiltonian equation below.

$$m\frac{d^2x}{dt^2} = -\frac{\partial H(x,t)}{\partial x} \quad 3.29$$

But since m is in atomic units, the dipole acceleration can be stated as;

$$\frac{d^2x}{dt^2} = -\frac{\partial H(x,t)}{\partial x}, \quad 3.30$$

which can simply be written as;

$$d_a t = -\frac{\partial H(x,t)}{\partial x} \quad 3.31$$

The average or the expectation value of this dipole acceleration is given by;

$$\langle d_a t\rangle = -\left\langle\psi(x,t)\right|\frac{\partial H(x,t)}{\partial x}\left|\psi(x,t)\right\rangle \quad 3.32$$

Where,

$$H(x,t) = T_{ion\,k} + V_{atm} + T_{el} + H_1 \quad 3.33$$

and T_{el} is the kinetic energy of electron, V_{atm} is the atomic potential, $T_{ion\,k}$ is the ion kinetic energy and H_1 is the atom-field interaction Hamiltonian term

While the electron is in motion due to the laser field, the atom is stationary and therefore the following relations holds;

$$T_{ion} = 0 \tag{3.34}$$

$$T_{el} = \frac{p^2}{2} \tag{3.35}$$

With these relations the Hamiltonian in eq.3.33 reduces to,

$$H(x,t) = V_s + T_{el} + H_1 \tag{3.36}$$

Where, V_s is the atomic potential. Therefore, in terms of a softcore parameter this can be written as;

$$V_s = -\frac{1}{\sqrt{x^2+a_0^2}} \tag{3.37}$$

Where a_0 is soft-core parameter. The reason for using the soft-core potential rather than the coulomb potential is to avoid getting infinite values at the origin. The soft-core parameter used in this thesis is 0.3282, a value that converges at the ground sate energy of hydrogen, $-0.5a.u$, as it will be shown in chapter four of this thesis.

To gather for atom-laser interaction, we introduced the atom interaction term which takes the form,

$$H_I = -xE(t) \tag{3.38}$$

as already stated in this chapter. Since this thesis employs the use of double IR laser pulse, it is important to note that the electric field $E(t)$ for the primary laser is given by;

$$E(t) = E_{01} f(t)\, cos(\omega t) \tag{3.39}$$

and the secondary laser it is expressed as;

$$E(t) = E_{02} f(t-\tau)\, cos(\omega(t-\tau) + \phi ce) \tag{3.40}$$

Where ϕce and τ are phase shift or Carrier Envelope Phase (CEP) and time delay between the primary and secondary lasers, respectively. All other terms still hold as used in the previous chapters of this thesis.

For the coupled lasers, the resulting laser field reads

$$E(t) = E_{01} f(t)\, cos(\omega t) + E_{02} f(t-\tau)\, cos(\omega(t-\tau) + \phi ce) \tag{3.41}$$

Where $f(t)$ is the temporal envelope of each IR pulse, E_{01} and E_{02} are amplitudes of the primary and secondary lasers, respectively.

If we consider the primary laser in eq.3.32 and associated Hamiltonian of the form;

$$H(x,t) = \frac{p^2}{2m} - \frac{1}{\sqrt{x^2+a_0^2}} - xE_{01}\, f(t)\, cos(\omega t) \tag{3.42}$$

The resulting equation is;

$$\langle d_a t\rangle t = -\left\langle \psi(x,t) \middle| \frac{d}{dx}\left[\frac{p^2}{2m} - \frac{1}{\sqrt{x^2 + a_0^2}} - xE_p\right] \middle| \psi(x,t)\right\rangle \tag{3.43}$$

Where E_p is the primary laser field.

After differentiating the inside square brackets eq.3.43 becomes,

$$\langle d_a t_p\rangle(t) = -\left\langle \psi(x,t) \middle| \frac{x}{x^2 + a_0^2} \middle| \psi(x,t)\right\rangle + E_p \tag{3.44}$$

The expectation value of dipole acceleration for secondary laser is given as;

$$\langle d_a t_s \rangle = -\left\langle \psi(x,t) \middle| \frac{d}{dx}\left[\frac{p^2}{2} - \frac{1}{\sqrt{x^2 + a_0^2}} - xE_s\right] \middle| \psi(x,t) \right\rangle \quad 3.45$$

Where, E_s is the secondary laser field.

Therefore, this equation can be written as;

$$\langle d_a t \rangle = -\left\langle \psi(x,t) \middle| \frac{x}{x^2 + a_0^2} \middle| \psi(x,t) \right\rangle + E_s \quad 3.46$$

For the two coupled or combined lasers,

$$\langle d_a t_c \rangle = -\left\langle \psi(x,t) \middle| \frac{x}{x^2 + a_0^2} \middle| \psi(x,t) \right\rangle + (E_c) \quad 3.47$$

3.4.2 HHG Spectrum Generated by an Ultrashort Laser Pulse

The HHG spectrum is obtained from the FFT of dipole acceleration, $d_a t$ [45]. FFT is a mathematical transformation that decomposes a function into frequency components [44]. This process of obtaining HHG Spectrum is given by eq.3.48.

$$HHG\omega = |\mathcal{F}\{d_a t\}|^2 \quad 3.48$$

Numerically, this is calculated as;

$$\hat{f}_1(\omega) = \frac{1}{\sqrt{2\pi}} \int_{-\infty}^{\infty} f(x) e^{-i\omega x} dx \quad 3.49$$

Where $\hat{f}_1(\omega)\ represent\ \langle d_a(\omega) \rangle$ and $f(x)\ represent\ \langle d_a(t) \rangle$. With these substitutions, eq.3.49 now reads;

$$\langle d_a(\omega)\rangle = \frac{1}{\sqrt{2\pi}}\int_0^{T_p} d_a(t)e^{-i\omega t}dt \qquad 3.50$$

Applying this on equations; eq.3.44, eq.3.45, and eq.3.47, we obtained the following equations;

$$\langle d_a(\omega_p)\rangle = \frac{1}{\sqrt{2\pi}}\left(\int_0^{T_p}\left[-\left\langle\psi\left|\frac{x}{x^2+a_0^2}\right|\psi\right\rangle\right]e^{-i\omega t}dt + \int_0^{T_p}[E_p]e^{-i\omega t}dt\right) \qquad 3.51$$

and

$$\langle d_a(\omega_c)\rangle = \frac{1}{\sqrt{2\pi}}\left(\int_0^{T_p}\left[-\left\langle\psi\left|\frac{x}{x^2+a_0^2}\right|\psi\right\rangle\right]e^{-i\omega t}dt + \int_0^{T_p}[E_c]e^{-i\omega t}dt\right), \qquad 3.52$$

respectively. These equations represent average dipole acceleration of electron in primary, i.e., single IR laser and coupled laser fields.

In the event that electron motion is controlled by a fundamental or the primary laser, single IR laser, the HHG spectrum is given by the equation;

$$HHG\omega_p = \left|\frac{1}{\sqrt{2\pi}}\left(\int_0^{T_p}\left[-\left\langle\psi\left|\frac{x}{x^2+a_0^2}\right|\psi\right\rangle\right]e^{-i\omega t}dt + \int_0^{T_p}[E_p]e^{-i\omega t}dt\right)\right|^2$$

$$= \left|\frac{1}{\sqrt{2\pi}}\left(\int_0^{T_p}\left[-\int dx\,\langle\psi(x,t)|x\rangle\,\frac{x}{x^2+a_0^2}\,\langle x|\psi(x,t)\rangle\right]e^{-i\omega t}dt + \int_0^{T_p}E_p dt\right)\right|^2 \qquad 3.53$$

$$= \left|\frac{1}{\sqrt{2\pi}}\left(\int_0^{T_p}\left[-\int dx\,|\langle x|\psi(x,t)\rangle|^2\,\frac{x}{x^2+a_0^2}\right]e^{-i\omega t}dt + \int_0^{T_p}E_p dt\right)\right|^2$$

While for the coupled or combined laser fields, the HHG Spectrum is given as;

$$HHG\omega_c = \left|\frac{1}{\sqrt{2\pi}}\left(\int_0^{T_p}\left[-\left\langle\psi\right|\frac{x}{x^2+a_0^2}\left|\psi\right\rangle\right]e^{-i\omega t}dt + \int_0^{T_p}[E_c]e^{-i\omega t}dt\right)\right|^2$$

$$= \left|\frac{1}{\sqrt{2\pi}}\left(\int_0^{T_p}\left[-\int dx\,\langle\psi(x,t)|x\rangle\,\frac{x}{x^2+a_0^2}\,\langle x|\psi(x,t)\rangle\right]e^{-i\omega t}dt + \int_0^{T_p}E_c dt\right)\right|^2 \qquad 3.54$$

$$= \left|\frac{1}{\sqrt{2\pi}}\left(\int_0^{T_p}\left[-\int dx\,|\langle x|\psi(x,t)\rangle|^2\,\frac{x}{x^2+a_0^2}\right]e^{-i\omega t}dt + \int_0^{T_p}E_c dt\right)\right|^2$$

Where $HHG\omega_p$ and $HHG\omega_c$ are high harmonic spectra for primary and coupled lasers, respectively. The results obtain from above equations of HHG spectra agree with the predictions of Three Step Model with slight This will be seen clear in chapter five but a simple example of this over estimation is shown below.

An example of harmonic spectrum for a hydrogen atom irradiated by a Ti: Sapphire laser pulse with a wavelength of 800 nm ($\omega = 1.55eV$) and a peak intensity of 1.6×10^{14}W/cm^{2}is shown in the **Fig 2:2**. The laser field *E(t)* was of the form, $E(t) = f(t)sin(\omega t)$, where the field envelope *f(t)* corresponds to a, 8-cycle flat-top pulse with a half-cycle turn-on and turn-off. It is clear that the spectrum has peaks at odd harmonic orders, as is experimentally observed, and the cutoff energy predicted by the cutoff law [46].

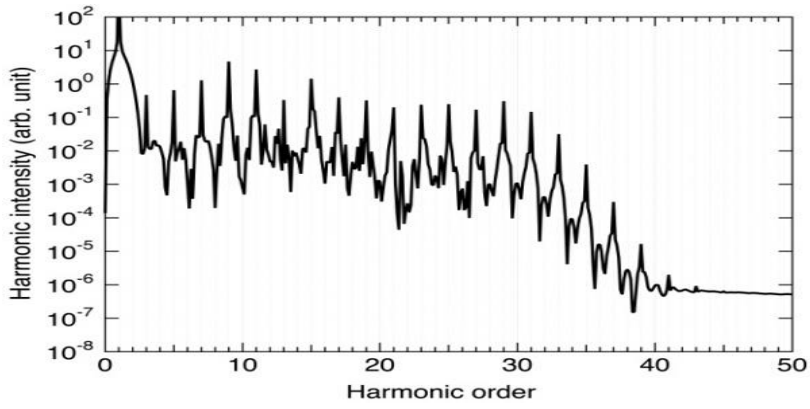

Fig 3:2 Experimental set up of Attosecond Pulse [18]

To prove the experimental results above, the calculation of the order of the cut off using eq.2.9 is necessary.

From quantum mechanics it is well known that energy is quantize, integer multiples of frequency, i.e., $E = n\omega$ where $n = 1, 2, 3, \ldots, N$. Therefore,

$$n\omega = I_p + 3.17U_p \qquad 3.55$$

from eq.2.8

$$U_p[eV] = {}^{I}/_{4\omega^2}$$

The atomic unit of laser intensity is

$$I_0 = 1a.u = \frac{1}{2}\varepsilon_0 cE^2 = 3.54 \times 10^{16} W.cm^{-2}$$

Hence, I in atomic units is;

$$I = \frac{1.6\times10^{14}}{3.54\times10^{16}} = 4.52 \times 10^{-3}$$

$$Up = \frac{4.52\times10^{-3}}{4(0.057)^2} = 0.3477$$

Substituting Up in eq.3.55 one gets;

$$n\omega = |I_p| + 3.17\ (0.3477\ )$$

And with $I_p = 0.5a.u$ and $\omega = 0.057a.u$, the Harmonic order *n* can be deduced as;

$$n = \frac{0.5+3.17(0.3477\ )}{0.057} \approx 33$$

This result, $n \approx 33$, approximately predicts the experimental results in the experimental one, $n \approx 32$ in **Fig 3:2**.

The ponderomotive potential associated with the field is the energy that the oscillating laser field can give to an electron in it. It is the energy of the propagating electron in the laser field. This energy is obtained through the real time propagation of the wavefunction as it will be described in the forthcoming chapter on results and discussions.

From the above, we have established how to obtain ponderomotive energy and to predict the experimental results of HHG spectrum using Three Step Model. Another important aspect discussed is the dipole acceleration which is the basis of computing HHG spectra.

Having described the laser-atom interaction, the next section is dedicated to bring insight of photons produced during the recombination process. In this work we considered a single and double IR laser pulses interacting with an atom simultaneously. The result of such interaction is a pulse in an attoseconds timescale. This pulse commonly known as Attosecond Pulse (ATP), is shown in **Fig 3:3** below.

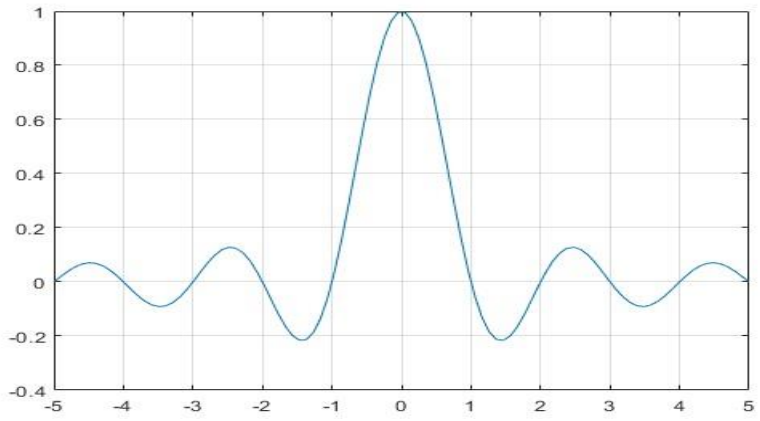

Fig 3:3 Temporal profile a Single Attosecond Pulse [31].

Chapter4 Attosecond Pulses

As discussed in chapter one, many applications of the Attosecond Pulse Train's (ATP) have been enabled by the availability of controlled attosecond pulses in form of XUVs. These pulses are either produced as Attosecond Pulse Train (APT) or Isolated Attosecond Pulse (IAP). To be able to produce these types of pulses using time delayed and identical IR pulses, it is necessary to first explore various methods.

The aim of this chapter is to provide insights on characterization and production of ATPs using double IR laser pulses, but as stated above, the following subsection is dedicated for exploring other methods used. Owing to some similarities with double IR pulses, the Two-color mixing is one of the methods described in detail [47].

4.1 Isolated Attosecond Pulse (IAP)

To observe electron dynamics in molecules and atoms on the attosecond timescale, single Isolated Attosecond Pulse (IAP) is utilized in performing pump–probe experiments. However, by manipulating the 3-step Model regimes; ionization, acceleration and recombination, many methods of generating IAP have been developed. These methods includes; Ionization Gating, where an IAP is generated by controlling the ionization process [47] and Polarization Gating, where the recombination process is manipulated through controlling displacement of electron due to polarization; if the displacement is so large the recombination is difficult [48, 49].

4.2 The Two-color Mixing

This method involves mixing of two lasers, a fundamental and a secondary laser, with different sets of parameters like wavelengths. By adjusting the wavelengths of these lasers, IAP can be generated through suppression of multiple pulse transient [50]. A secondary laser field of a lower wavelength has a constructive interference at the second or third peak when mixed with the fundamental field. Unfortunately, this kind of wavelength for a secondary laser does not favour the generation of a broader plateau. Therefore, a secondary laser field of a higher wavelength tend to be used [51].

4.2.1 Essential Conditions of a Driving Laser Field for Creating IAP

As explained in chapter two, High-order Harmonic Generation (HHG) is due to recombination process of an electron and its parent ion. This process happens within half cycle of oscillating electric field, where, electron leaves and accelerates back in the continuum to its parent atom. However, when a multicycle laser field is used instead, the temporal structure of the harmonics will see a pulse train formation. Therefore, to create IAP, it is necessary to confine the driving laser field to a few optical cycles of around $5\,femtoseconds\,(ft)$ or less, $T_p < 5\,femtoseconds\,(ft)$ [52]. When the pumping pulse have a few-cycle electric field, the photon energy near the cut-off region of HHG can be confined to one half of the electric field at the central peak [53]. Therefore, by extracting the cut-off components of the high harmonics beam, it is possible to obtain an IAP.

As mentioned in chapter two, the deterministic factors of this pulse, i.e., the Carrier Envelop Phase (CEP) and electric field $E(t)$ at time t are given by the relation;

$$E(t) = E_1 e^{-2ln\left(\frac{t}{\tau_0}\right)^2} cos(\omega_1 t + \phi ce) \tag{4.1}$$

With regards to double IR pulses, this relation can be modified to;

$$E(t) = E_2 e^{-2ln\left(\frac{t}{T}\right)^2} cos(\omega_2 t + \phi ce) + E_2 e^{-2ln\left(\frac{t-\tau}{T}\right)^2} cos(\omega_2 t + \phi ce) \tag{4.2}$$

Where, τ is the delay time between the main field laser and the supplementary or secondary field laser and ϕce is the phase shift. The other terms still hold as previously used.

When ϕce changes shot by shot, the structure of the electric field also changes. This effect leads to the generation of Attosecond Pulse Train (APT). A prototypical example of APT is displayed in ***Fig 4:1***.

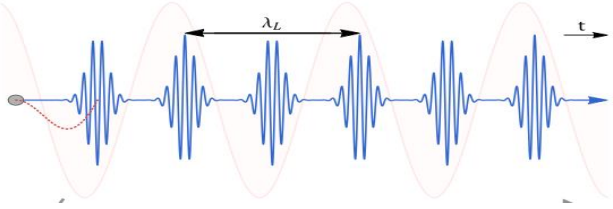

Fig 4:1 Attosecond Pulse Trains (APT) [31].

4.2.2 Continuum Analysis

This analysis is fundamental for the optimization of the laser wavelengths in Two Color (TC) mixing. The ratio R of the TC field is defined as;

$$R = \frac{E_{1st}}{E_{2nd}} \tag{4.3}$$

Where E_{1st} denotes the strongest amplitude of the TC field, while E_{2nd} denotes the second strongest amplitude. Another important factor considered during this analysis is the intensity difference ratio δ_d, which is defined as;

$$\delta_d = \frac{{E_{1st}}^2 - {E_{2nd}}^2}{{E_{1st}}^2} \tag{4.4}$$

The two ratios, R and δ_d, are bounded by the fact that large values of R results in greater values of δ_d. This fact leads to a longer continuum length thereby creating a shorter attosecond pulse duration [52]. The importance of this relation is that it helps determine the type of colors used as components of the TC field.

Due to the availability of 800nm laser, the wavelength of the first color field is fixed at 800nm. Depending on the fact that longer driving wavelengths extends the cut-off [54] and decreases the efficiency of HHG process [55], the wavelength ranging from 300nm to 2800nm tend to be used as the second color field laser. An example on how electric field changes in TC mixing is shown in **Fig 4:2**

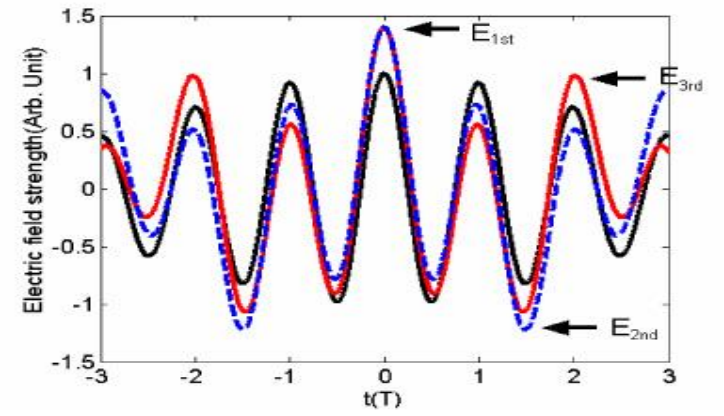

Fig 4:2 The Electric Field of Single and Mixed Laser field [31]

In **Fig 4:2**, E_{1st}, E_{2nd} and E_{3rd} are in order of strongest to the least electric field peak, respectively.

Having briefly described how to generate an attosecond pulse by Two-color mixing, the next section introduces the methodology of generating ATP using double IR pulse.

4.3 Methodology

This section is purposely for building up all the required parameters and procedures for a successful simulation of our results. When the induced femtosecond laser interacts with the Hydrogen H atom, it ionizes forcing detachment of the electron. This electron is accelerated in continuum by electric field which is reinforced by identical secondary laser. Eventually this electron recombines with the parent atom. To study this recombination process, we ran a simulation for the emission spectra.

Before running the simulation, we start with the process of modelling an environment that will act as defining modulators of our propagation. This consists of the momentum space that describes electron kinetic energy in the continuum, the position space that describes the position of the electron wave packet and time grid that describes instantaneous time of electron.

4.3.1 Position Grid

The grid size L_x, along the electronic coordinates was designed to allow full oscillation of electron in the electric field. Here we chose $L_x = 7$ to represent the maximum range from -2α to 2α, where $\alpha = 1.0$

The length L, therefore, becomes;

$$L = 2\pi L_x \tag{4.5}$$

By letting the boundary positions to be X_{min} and X_{max} or $-\frac{L}{2}$ and $\frac{L}{2}$, respectively, the position at any instant is given by;

$$X_n = X_{min} + n\Delta x \tag{4.6}$$

With *n (points) = 0, ...,* $N_x - 1$, N_x is the total grid points (86 points) and Δx is the electronic spacing.

4.3.2 Momentum Grid

The momentum was defined as $-p_{max}$ and p_{max} representing minimum and maximum momenta, respectively. In terms of electronic spacing, these momenta were given as;

$$p_{max} = \frac{\pi}{\Delta x} \tag{4.7}$$

and

$$p_{min} = -\frac{\pi}{\Delta x} \tag{4.8}$$

At any point, momentum *p* is given by;

$$p_i = p_{min} + n\Delta p \tag{4.9}$$

With $p_{min} = -p_{max}$, momentum spacing $\Delta p = \frac{p_{max} - (-p_{max})}{N_x}$. It is also important to note that the momentum grid was split into two lines, one that is going from $-p_{max}$ to *0* and from 0 to p_{max}. This is because we have two maxima with both having *0* as p_{min}.

4.3.3 Temporal Grid

We considered different temporal grids, the imaginary time propagation, the real time propagation and the time for spectrum computation.

In real time space we used the number of timesteps N_t , of 1600 and 4800. With the time grid size of [*0*, t_{max}], the timestep $\Delta t = \left(\frac{t_{max}}{N_t}\right)$. Therefore, time in real space is given by;

$$t = t_0 + k\Delta t \tag{4.10}$$

where $k = 0, 1, 2, \ldots, N_t - 1$ *and* $t_0 = 0$.

In the imaginary time propagation, we set $t \longrightarrow -it$ and $\Delta t \longrightarrow -i\Delta t$. Therefore, the imaginary time is given by;

$$t = t_0 - ik\Delta t \tag{4.11}$$

where i is complex number.

It is important to note that this imaginary time propagation will be used in the simulation of ground state energy of the system, the hydrogen atom.

4.4 Absorbing Barriers

Since the wavefunction is too large, we set an absorbing barrier in such a way that it confines this wavefunction and prevents its reflection and reentering of ghost wavefunction at the endpoints of the spatial grid. This absorbing barrier is a potential added to the laser for damping action of the electron motion near the grid boundaries.

Here, we used an optical barrier of the form;

$$V_{opt} = -i\left[\theta(x - x_1)\left(\frac{x - x_1}{x_{max} - x_1}\right)^2 - \theta(x_2 - x)\left(\frac{x - x_2}{x_{min} + x_2}\right)^2\right] \tag{4.12}$$

Where $x_1 = x_{max} - \frac{5\pi L_x}{10}$, $x_2 = x_{min} + \frac{5\pi L_x}{10}$, and θ is the Heaviside function controlling the absorption of the wavefunction.

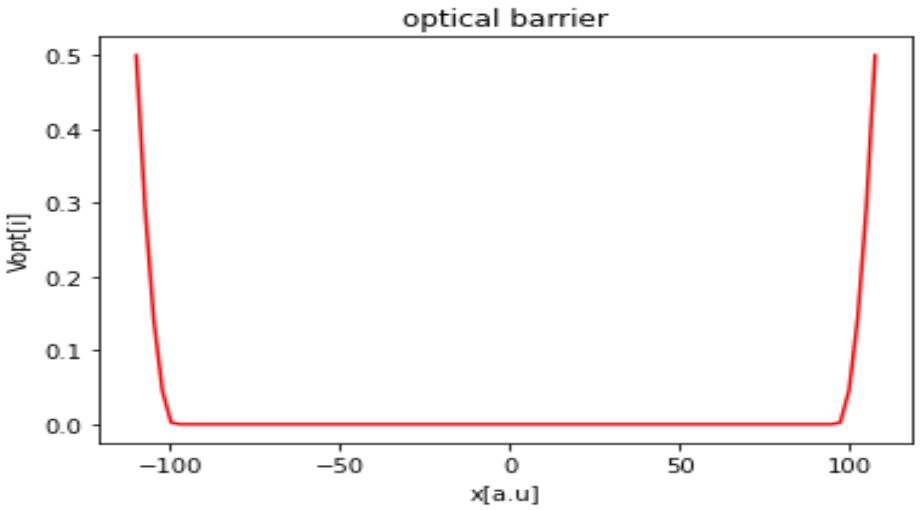

Fig 4:3 Potential Barrier

This Heaviside function, usually set to 0.5, must not be too large to allow reflection of the wave packet and at the same time not too small to permit reentering of a ghost wave packet. Therefore, it is important to note that this potential is imaginary and is added to the laser potential for damping action of electron approaching grid boundaries.

4.4.1.1 Soft-core Coulomb Potential

Normally, the coulomb potential of hydrogen H atom is given as;

$$V = -\frac{e}{4\pi\epsilon_0 x} \tag{4.13}$$

In atomic units this equation can simply be stated as;

$$V = -\frac{1}{x} \tag{4.14}$$

But in order to avoid singularity at the origin, we introduced a soft-core parameter modifying this potential as a softcore potential of the form;

$$V_{soft\ core} = -\frac{1}{\sqrt{x^2 + a_0^2}} \quad 4.15$$

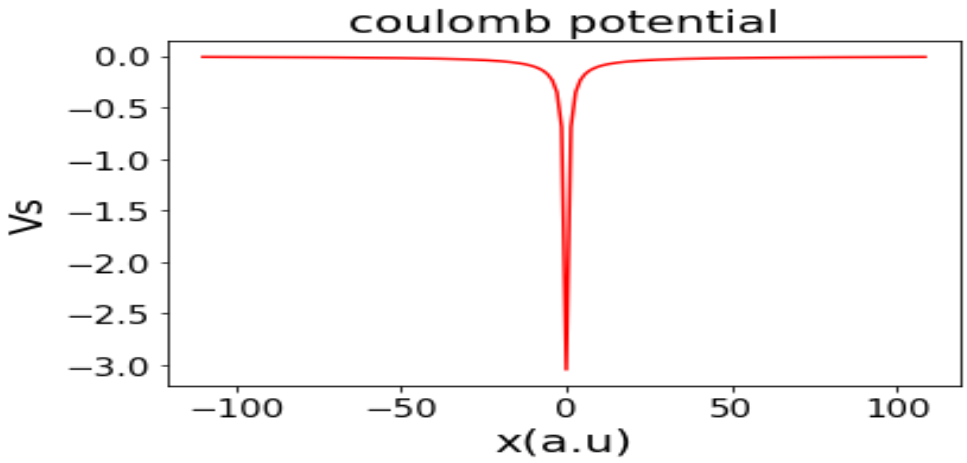

Fig 4:4 Soft-core Coulomb Potential.

Where a softcore parameter a_0, is set to 0.3282. Besides being chosen to avoid singularity of potential at the origin, at $x = 0$, this parameter makes the system converge at the Ground State Energy $E_g = -0.5a.u$, which is exactly the ground state energy for hydrogen H atom. Moreover, a_0 has been verified to have some significance on plateau where, smaller values of this soft-core parameter give rise to broader plateau, as compared to larger values [64].

4.4.2 Gaussian Potential

For the purpose of comparison with the Softcore Coulomb potential we considered the Gaussian potential of the form

$$V(x) = -1.1exp(-x^2/\sigma^2) \quad 4.16$$

where σ^2 is gaussian parameter.

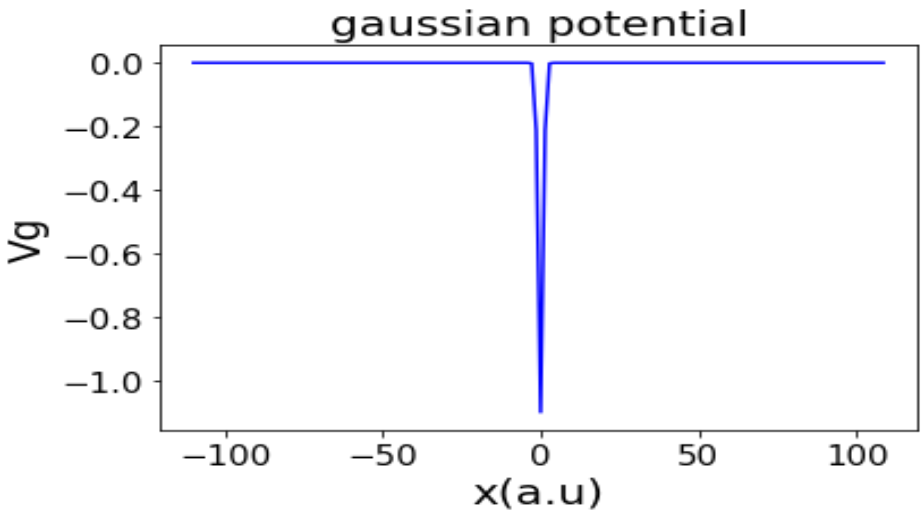

Fig 4:5 Gaussian Potential with $\sigma^2 = 1.21$

The Gaussian potential has only a single bound-state unlike the soft-core coulomb potential which allows for a Rydberg series.

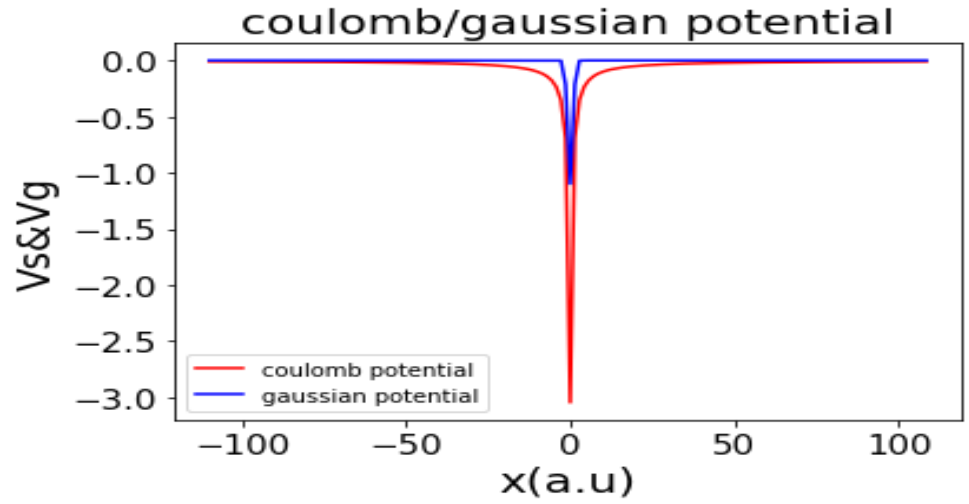

Fig 4:6 Gaussian and Coulomb Potential**.**

This is shown clearly in **Fig 4:6**. Both potentials did not change over widely spread grid since the potentials could only depend on the choice of coulomb and gaussian parameters used.

4.4.2.1 Imaginary Time Propagation of The Wavefunction

The initial wavefunction was chosen to take the gaussian form in eq.4.17.

$$\psi(x,0) = e^{-\frac{\alpha x^2}{2}} \tag{4.17}$$

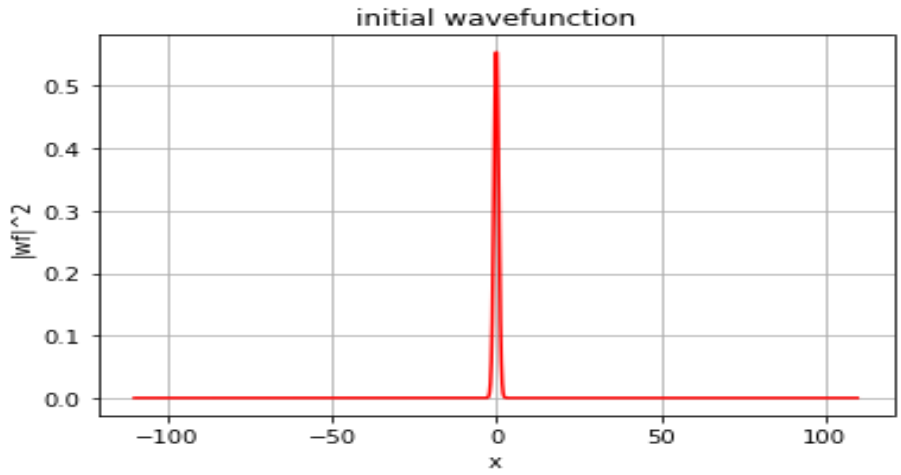

Fig 4:7 Normalized Initial Wavefunction with higher Spatial Grid points.

This ***Fig 4:7*** shows that the electron was initially at the origin with the probability of 0.55.

Having defined the atomic and barrier potential, the total potential now takes;

$$V \rightarrow V_{soft\ core} + V_{opt} \tag{4.18}$$

This potential was used in computation of the ground state energy of the system, H atom. The ground state energy is obtained when the imaginary time propagation is converged, that is when the energy does no longer changes. Therefore, as stated before,

$$\Delta t \rightarrow -i\Delta t \tag{4.19}$$

Hence, eq.3.13 becomes;

$$\psi_{img}(x,t) = e^{-\frac{V}{2}\ \Delta t} e^{-\hat{T}\,\Delta t}\ e^{-\frac{V}{2}\ \Delta t} e^{-\frac{\alpha x^2}{2}} \tag{4.20}$$

Where $\psi_{img}(x,t)$ is the imaginary time propagated wavefunction.

Since the propagting wavefunction hoops between the real and momentum space, we perfomed the action of eq.3.14 to eqn.3.18 on eq.4.20 and the result is the normalized wavefunction shown in ***Fig 4:8*** below.

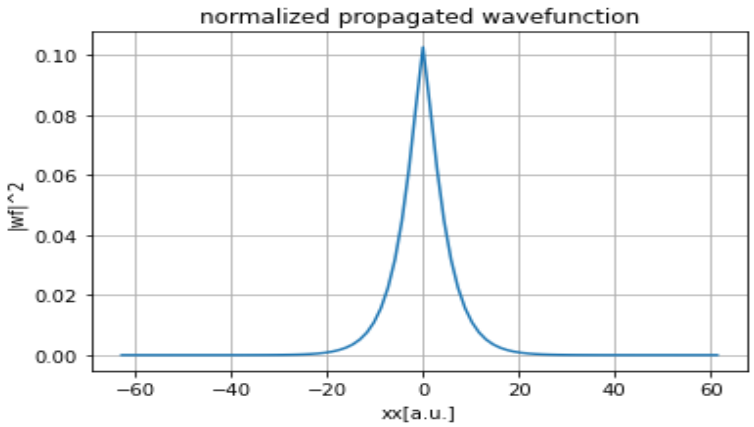

Fig 4:8 Propagated Wavefunction.

The **Fig 4:8** shows that after relaxing the system through imaginary time propagation, the probability of the electron being at the origin is 0.10

It is clear that initial and propagated wavefunctions have different probabilities of electron being at the origin. This is shown in **Fig 4:9** below.

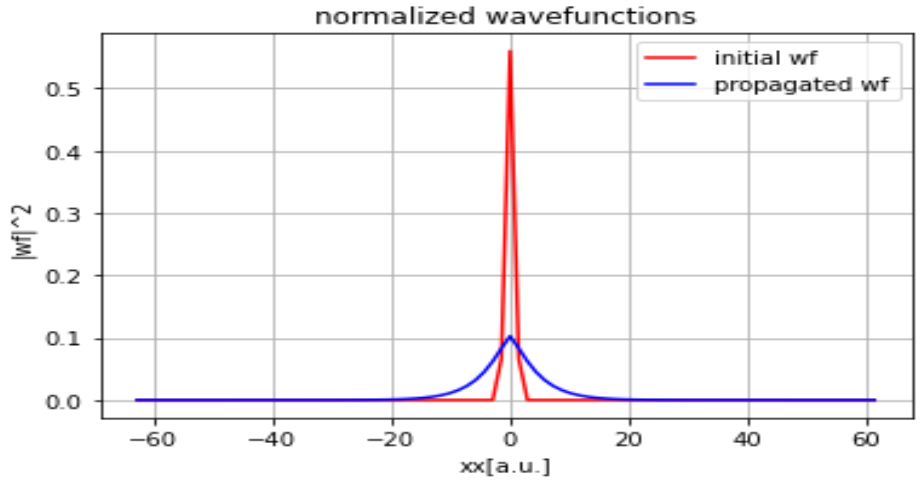

Fig 4:9 Both Initial (red) and Propagated (blue) Wavefunctions.

In **Fig 4:9**, the red line represents the initial wavefunction with the probability of finding an electron at the origin being 0.55. When this wavefunction is propagated through imaginary time, we obtained the propagated wavefunction in blue with the probability of finding an electron at the origin dropping to 0.1. Because it suffers less dumping compared to initial wavefunction, the propagated wavefunction results in the ground state energy in **Fig 4:10**.

4.4.2.2 Ground State Energy

This is the initial state of our computation i.e., obtaining the ground state of system. This can also be referred to as the ionization energy of the H atom. As stated above, this computation is done through the imaginary time propagation.

We computed the kinetic and potential energy of the H electron by using eq.3.21 and eq.3.27. Therefore, the ionization energy, I_p now reads;

$$I_p = \langle E_{kin} \rangle + \langle E_{pot} \rangle \tag{4.21}$$

I_p now represents the total energy of the electron in **Fig 4:10** below. The plot shows that indeed the atomic species is H atom.

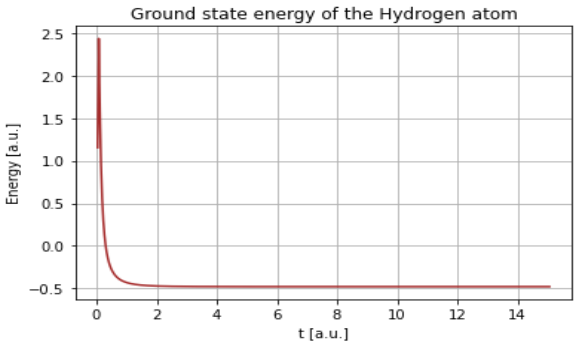

Fig 4:10 Energy of the system as a function of time t.

In **Fig 4:10**, the electron's initial energy was approximately 2.5a.u, but after about 2a.u time of propagation the system was well relaxed. Hence, we obtained the Ground State Energy of $-0.5a.u$ which indeed corresponds to Ground State Energy of H atom. As discussed before, the choice of the soft-core parameter i.e., 0.3282 was significant in ensuring convergence of energy at $-0.5a.u$.

4.4.3 Laser Irradiation

The coupled laser field takes the form;

$$E(t) = E_1 f(t) sin(\omega_1 t - \phi ce) + E_2 f(t) sin(\omega_2 (t + \tau) - \phi ce)), \tag{4.22}$$

and the characteristics of the two lasers used as are given below.

Primary Laser

As discussed in chapter three primary laser had the form;

$$E(t) = E_1 f(t) sin(\omega_1 t - \phi ce) \quad 4.23$$

Where $f(t) = cos^2\left(\frac{t}{T_p}\right)$ is the envelope, $T_p(pulse\ duration) = \text{nc}_1 \times \text{T(pulse length)}$, $\omega_1 = \frac{2\pi c}{\lambda_1}$, $T = \frac{2\pi}{\omega_1}$ and $E_1 = \sqrt{\frac{2\times I}{\varepsilon_0 c}}$.

Primary laser had the following specific characteristic parameters;

Intensity I	$\mathbf{2 \times 10^{14} W/cm^2}$	0.0057a.u
Wavelength $\boldsymbol{\lambda_1}$	800nm	0.057a.u
Optical cycles $\mathbf{nc_1}$	10 optical cycles	10

$E_1 = \sqrt{\frac{2\times 10^{14}}{3\times 10^{16}}}$

Secondary Laser

$$E_2 f(t) sin(\omega_2(t+\tau) - \phi ce)) \quad 4.24$$

Secondary laser is the replica of the primary laser and had same characteristics has shown below.

Intensity I	$\mathbf{2 \times 10^{14} W/cm^2}$	0.0057a.u
Wavelength $\boldsymbol{\omega_1}$	800nm	0.057a.u
Optical cycles $\mathbf{nc_1}$	10 optical cycles	10

Here $\text{E}_2 = \text{E}_1$

Here, ϕce was zero and the results were obtained different values of τ ,i.e., 0.0a.u, 400a.u and 1250a.u.

After defining the atomic environment and the ground state energy of the system, the following subsection gives the wavefunction with a redefined system potential.

4.4.3.1 System Potential

For the next sections we took into consideration the laser potential and now potential reads;

$$V \rightarrow V_{soft\ core} + V_{opt} + V_{laser\ potential} \tag{4.25}$$

Unlike potential in eq.4.18, this potential accounts for laser-atom interaction by including $V_{laser\ potential}$.

4.4.3.2 Real Time Propagation

The real time propagation of the wavefunction is essential for simulating the energy of the accelerating electron. This wavefunction takes the form of eq.4.26 shown below.

$$\psi(x, t + \Delta t) = e^{-\frac{V}{2}i\Delta t} e^{-Ti\Delta t} e^{-\frac{V}{2}i\Delta t} \Psi_{img} \tag{4.26}$$

Where $\psi(x,t)$ is the real time propagated wavefunction and Ψ_{img} the initial wave function or the ground state wave function resulting from the imaginary time propagation.

We then performed the action of eq.3.14 to eq.3.18 of the Split Operator Method to simulate the result of eq.4.26.

Chapter5 Results and Discussions

5.1. Energy of an Accelerating Electron

After ionization, the electron accelerates in the continuum attaining energy commonly known as the ponderomotive energy U_p. This energy is influenced by the laser field under which an electron oscillates. In this work we considered three kinds of laser fields: (i) a single IR laser field, (ii) a delayed double IR laser field, and (iii) a non-delayed double IR laser field.

This energy can be computed through the real time propagation of wavefunction. Therefore, the total energy of electron in the oscillating field is given as;

$$E_{total} = U_p = \langle E_{kin} \rangle + \langle E_{pot} \rangle \quad 5.1$$

Where U_p now represent the energy of accelerating electron.

Starting with the first case where the atom is in a Single IR laser field, the energy of an accelerating electron is shown in **Fig 5:1**.

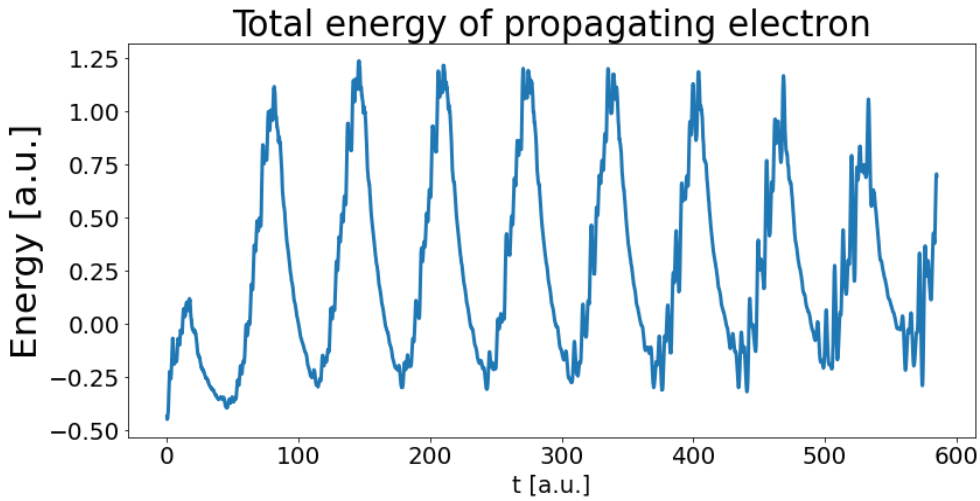

Fig 5:1 Energy of Accelerating Electron due to a Single Laser Field.

From **Fig 5:1**, it is clear that after ionization, - 0.5a.u, accelerating electron attained an average energy of 1.25a.u.

For the second case where the atom is in a non-delayed double IR laser field, the energy of accelerating electron is shown in **Fig 5:2**.

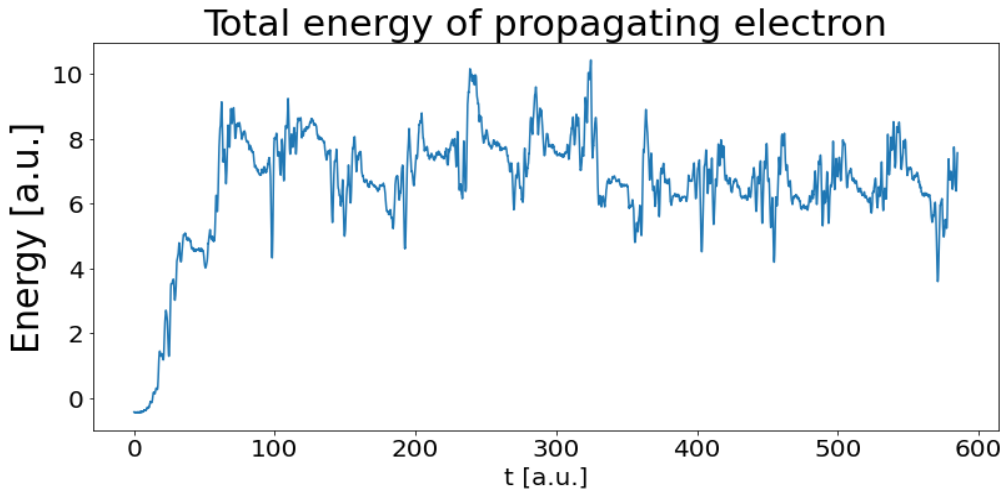

Fig 5:2 Energy of Accelerating Electron due to Douple IR Pulse.

From **Fig 5:2** above, it is clear that after ionization, - 0.5a.u, the electron gained energy up to an average energy of 8a.u. Here, it is important to note that the two laser pulses were coupled with no time delay.

Considering the third case where the atom is in a delayed double IR laser field, the energy of the propagating electron is shown in **Fig 5:3** below. It is important to note that this plot was computed with time delay of $\tau = 300$ a.u.

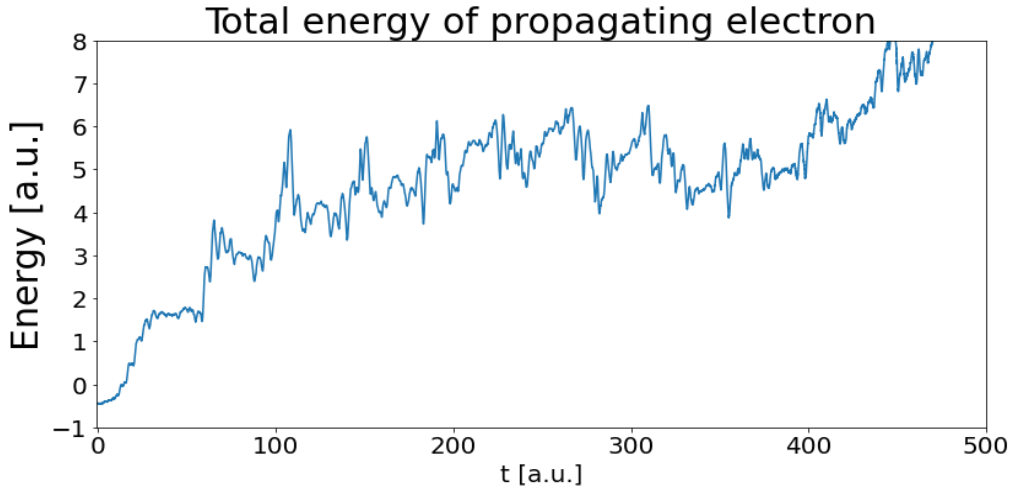

Fig 5:3 Energy of Accelerating electron due to 2 Replica IR with $\tau = 300\ a.u.$

After ionization the electron attained an average energy of 6 a.u. as shown in **Fig 5:3**. Unlike the delayed IR laser field, the non-delayed IR laser field is reinforced by the two laser fields which are in phase.

5.2. Dipole Acceleration

As explain in chapter three, to understand the dynamics of the recombination process, we have to study the emission spectrum, HHG Spectrum. The basis of this spectrum is the dipole acceleration.

Just like in the case of computing energy of accelerating electron, the dipole acceleration depends on the laser field. Therefore, we considered three cases, as used above: (i) a single IR laser field, (ii) a delayed double IR laser field, and (iii) non-delayed IR laser fields.

By considering the first case here dipole acceleration due to single IR pulse, the dipole acceleration was computed using eq.3.44 which was stated as;

$$\langle d_a t_p \rangle = -\left\langle \psi(x,t) \middle| \frac{x}{x^2 + a_0^2} \middle| \Psi(x,t) \right\rangle + E_p$$

The result of this computation is shown in **Fig 5:4** below.

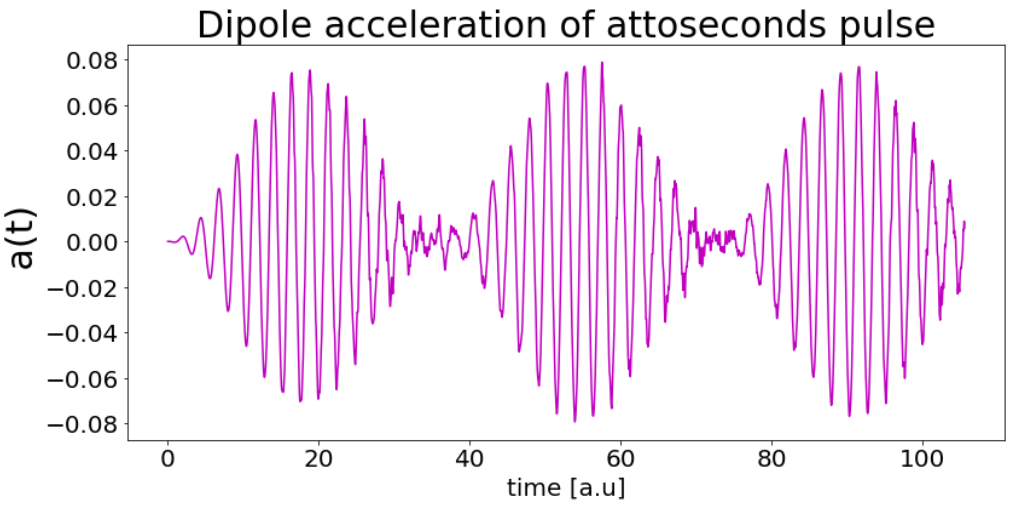

Fig 5:4 Dipole Acceleration of Single IR Laser Pulse.

In **Fig 5:4**, each of the three pulses has a duration of about 35a.u. This single pulse's duration is clearly shown in **Fig 5:5** below.

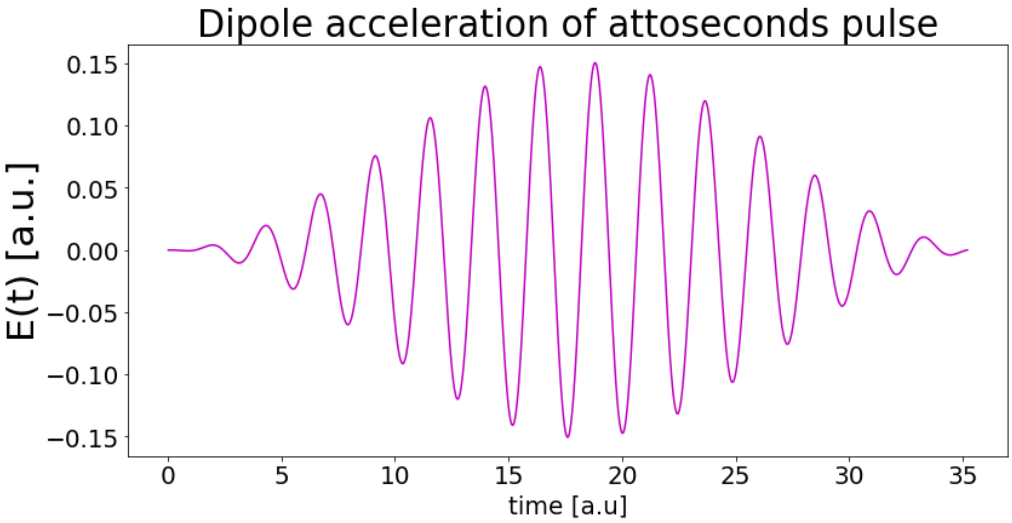

Fig 5:5 Dipole Acceleration of Single IR Pulse.

The second case uses the non-delayed double IR laser field. The dipole acceleration due to this field was computed using eq.3.46 which states;

$$\langle d_a t_c \rangle = -\left\langle \psi(x,t) \middle| \frac{x}{x^2 + a_0^2} \middle| \psi(x,t) \right\rangle + E_c$$

The result of this computation is shown in **Fig 5:6** below.

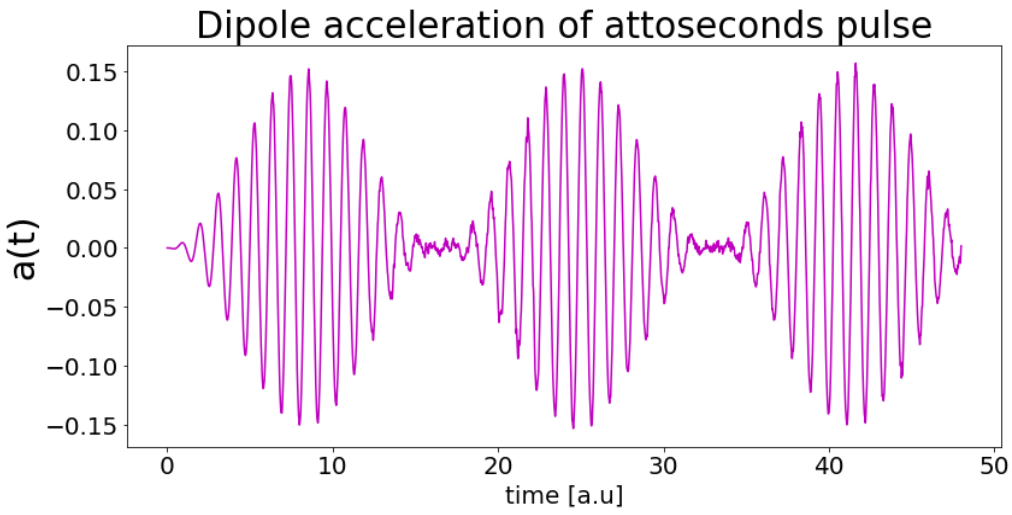

Fig 5:6 Train of Pulses of Dipole Acceleration of Double replica IR Laser Pulse.

Each pulse in **Fig 5:6** has a duration of 16a.u as clearly shown in **Fig 5:7**.

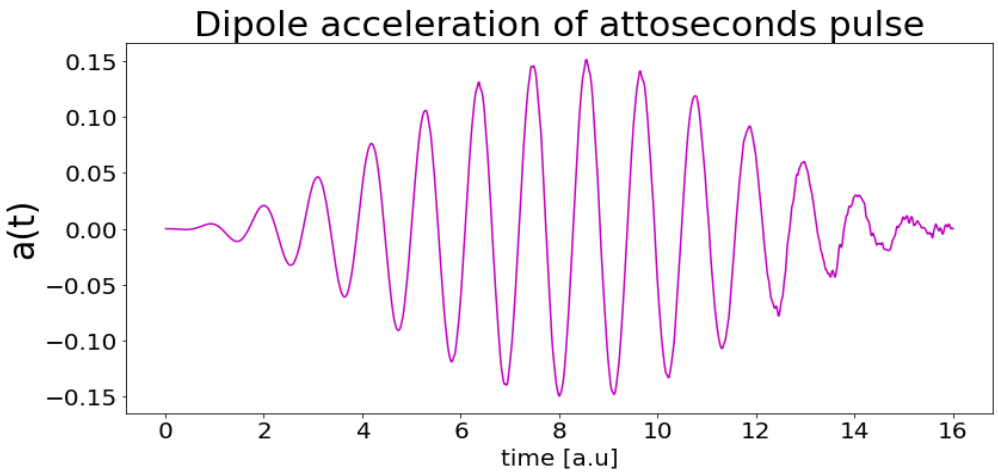

Fig 5:7 A Single Pulse due to a Double Laser.

Form the above computation, it is clear that a short pulse with a pulse duration of 16a.u is produced when double IR laser field is used. On the other hand, when a single IR laser field is used, a pulse with a pulse duration of 35a.u is produced. This is clearly shown in **Fig 5:7** and **Fig 5:5**, respectively.

For a delayed double IR laser with time delay of $\tau = 400a.u$ and $\tau = 1250a.u$, the dipole accelerations are shown in **Fig 5:8** and **Fig 5:9**, respectively.

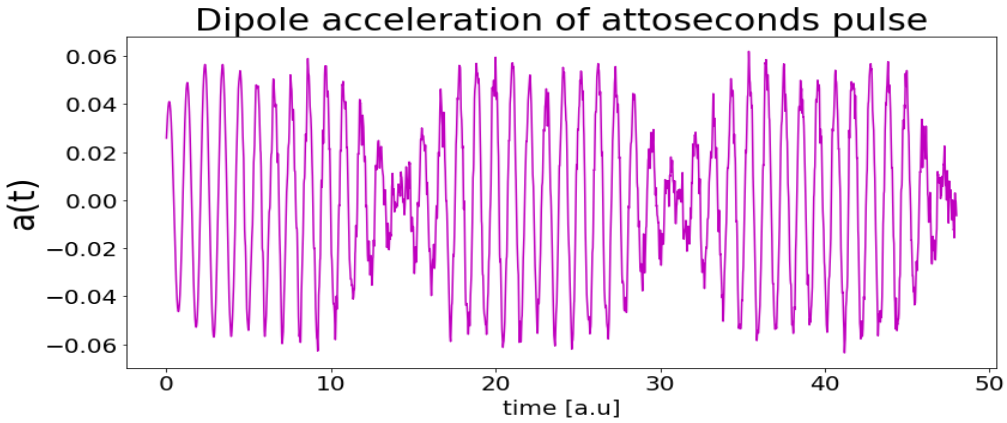

Fig 5:8 A Dipole Acceleration from Double IR Laser with $\tau = 400a.u.$

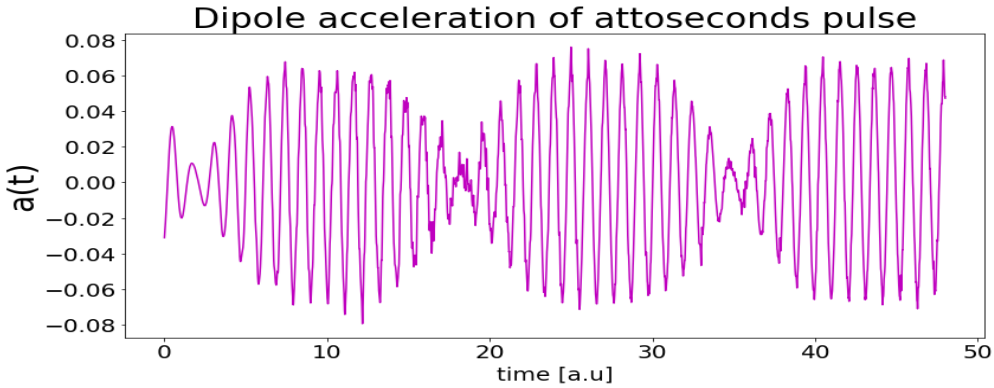

Fig 5:9 A Dipole Acceleration from Double IR Laser with $\tau = 1250a.u.$

Even though the two plots have the same amplitudes, there is less phase mismatch in **Fig 5:9** than in **Fig 5:8**.

After computing the basis, dipole acceleration, the next section will be for the computation of HHG spectra.

5.3. HHG Spectra

The HHG spectrum gives insights of the recombination process and is obtained by taking FFT of dipole acceleration. This work utilizes the dipole accelerations obtained above. It is important to note that in the previous section we used three cases of laser field, namely (i) a single IR laser field, (ii) a delayed double-delayed and (iii) a non-delayed double IR laser field.

For the single IR laser field, the FFT of dipole acceleration is given by eq.3.51 as:

$$HHG\omega_p = \left| \frac{1}{\sqrt{2\pi}} \int_0^{T_p} \left[- \left\langle \psi(x,t) \middle| \frac{x}{x^2 + a_0^2} \middle| \psi(x,t) \right\rangle \right] e^{-i\omega t} dt + \int_0^{T_p} E_p e^{-i\omega t} dt \right|^2$$

This computation resulted in HHG spectrum shown in **Fig 5:10** and **Fig 5:11**.

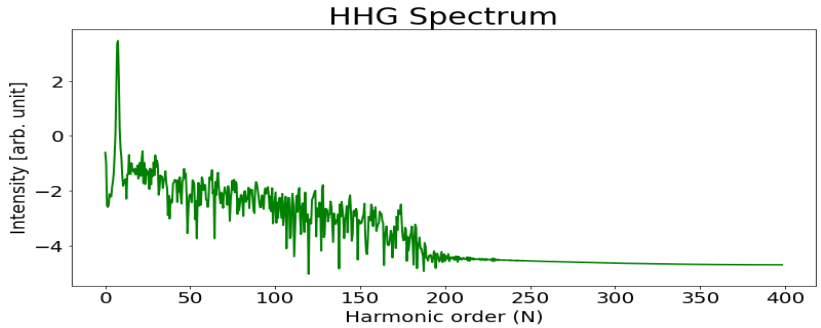

Fig 5:10 HHG Spectrum due to a Single IR Pulse, computed with 1600 grid points.

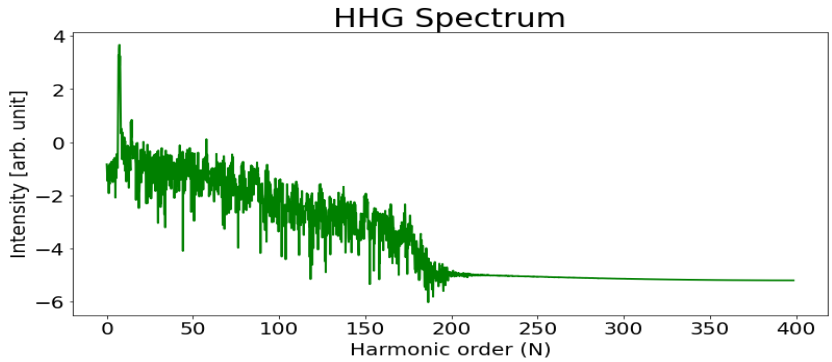

Fig 5:11 HHG Spectrum due to a Single IR Pulse, computed with 4800 grid points.

The two figures, **Fig 5:10** and **Fig 5:11**, were plotted with 1600 and 4800 points, respectively. The HHG spectra reveal that the harmonics of up to 78th order were produced when a single IR laser pulse was used. This implies that during recombination, photons of very high frequencies were emitted. These frequencies were 78 times the absorbed frequency. Using the Three Step Model, these results can be predicted as;

$$Energy = I_p + 3.17U_p$$

$$Energy = n\omega$$

$$n = \frac{|I_p| + 3.17(U_p)}{\omega}$$

$$U_p = 1.25a.u \; and \; I_p = 0.5a.u$$

$$n = \frac{0.5 + 3.17(1.25)}{\omega} = \frac{4.4625}{0.057} = 78.3$$

This harmonic order can be converted to the corresponding energy in *eV* using the equation;

$$energy(eV) = \omega \times 27.211eV \times n \qquad 5.2$$

Therefore, 78th order is equivalent to 120eV.

The harmonic order of 78th, obtained from the HHG spectrum of **Fig 5:11** is very close to predicted one (78.3th), calculated using the formula in eq. 5.2 above.

The HHG spectrum due to double IR laser pulse is govern by eq.*3.51* and can be stated as;

$$HHG\omega_c = \left| \frac{1}{\sqrt{2\pi}} \int_0^{T_p} \left[- \left\langle \psi \right| \frac{x}{x^2 + a_0^2} \left| \psi \right\rangle \right] e^{-i\omega t} dt + \left(\int_0^{T_p} E_c e^{-i\omega t} dt \right) \right|^2$$

The result of this computation is depicted in **Fig 5:12** below with 0.0a.u time delay between the two double IR laser of 15 optical circles each.

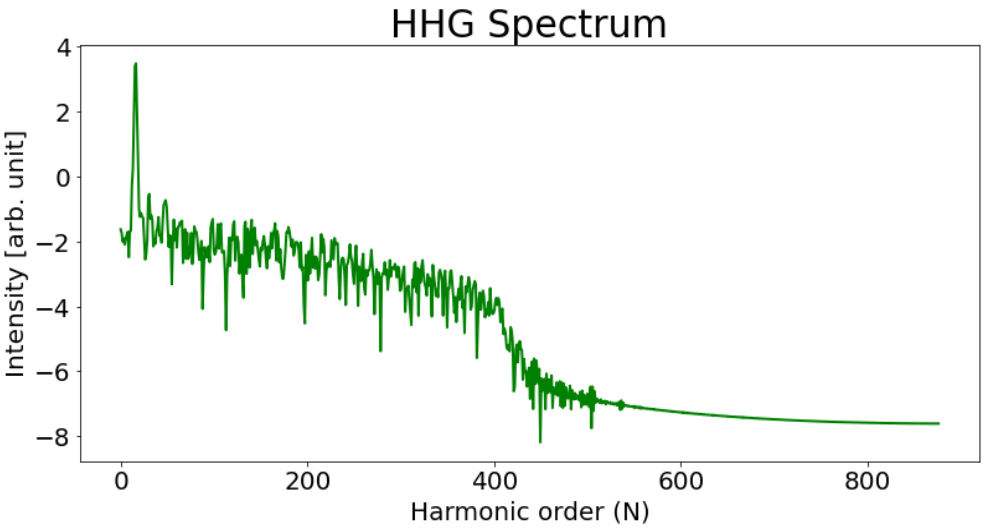

Fig 5:12 HHG Spectrum due to Double IR Lasers.

The cutoff energy in **Fig 5:12** is at harmonic order of 400. This implies that the emitted photons are 400 times the absorbed frequency. This frequency is so high as compared to that of emitted photons due to single laser field interaction with the H atom.

This harmonic order due to double IR laser field can be predicted by Three Step Model as;

$$Energy = I_p + 3.17U_p$$

$$n = \frac{|I_p| + 3.17(U_p)}{\omega}$$

$$U_p = 8\ a.u\ and\ I_p = 0.5\ a.u$$

$$n = \frac{0.5 + 3.17(8)}{\omega} = \frac{25.86}{0.057} = 453.6$$

This value is approximately close to that obtained from the HHG spectrum in **Fig 5:12**. Using eq.5.2, the corresponding energy of this harmonic order is $700eV$;

The plateau in **Fig 5:12** runs from 40^{th} to 400^{th} order and is computed with 1600 grid points. However, the plateau is well resolved with more grid points, say 4800, as illustrated in **Fig 5:13** below.

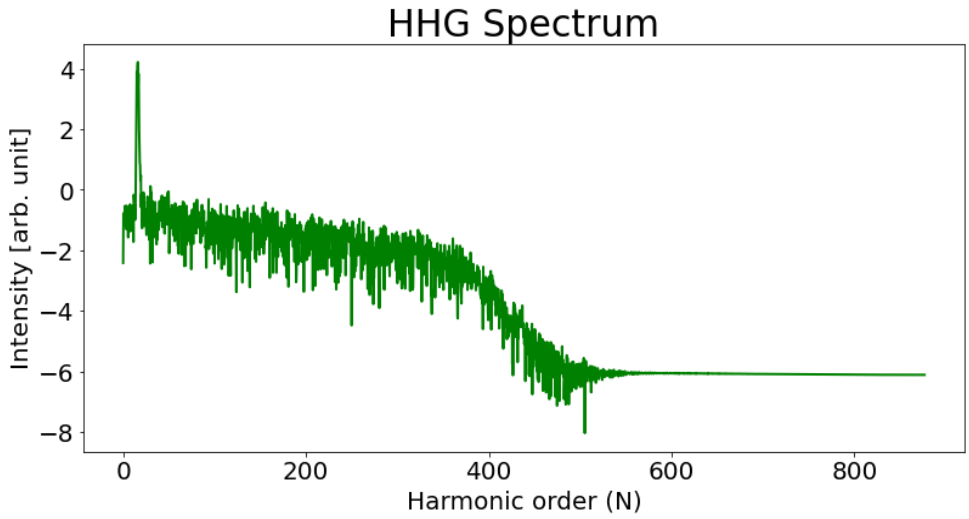

Fig 5:13 HHG Spectrum of H atom due to Double IR Lasers.

This number of grid points only affects the resolution of the plateau and not the cut off energy.

In this work one of the main factors considered when computing these results was time delay. Therefore, the following section is solely for comparing results obtained from different time delays. In terms of dipole acceleration which is the basis of HHG spectrum, the plots of the three different time delays are shown in **Fig 5:14** below.

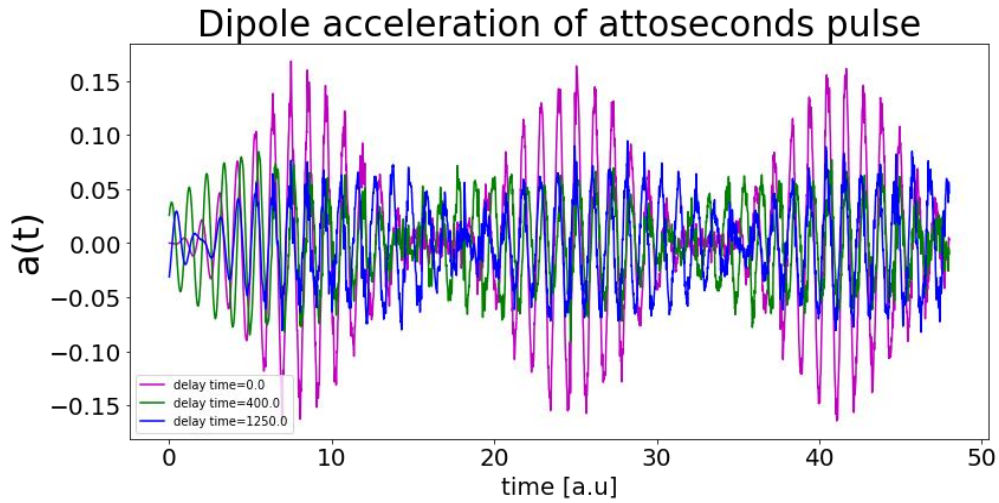

Fig 5:14 Dipole Acceleration due to Different Time Delays.

The purple, the blue and the green represent the dipole acceleration for 0.0 a.u., 400a.u. and 1250 a.u. time delays between the driving lasers, respectively. Taking the associated FFT of the dipole acceleration above, the resulting HHG spectra are depicted in **Fig 5:15**.

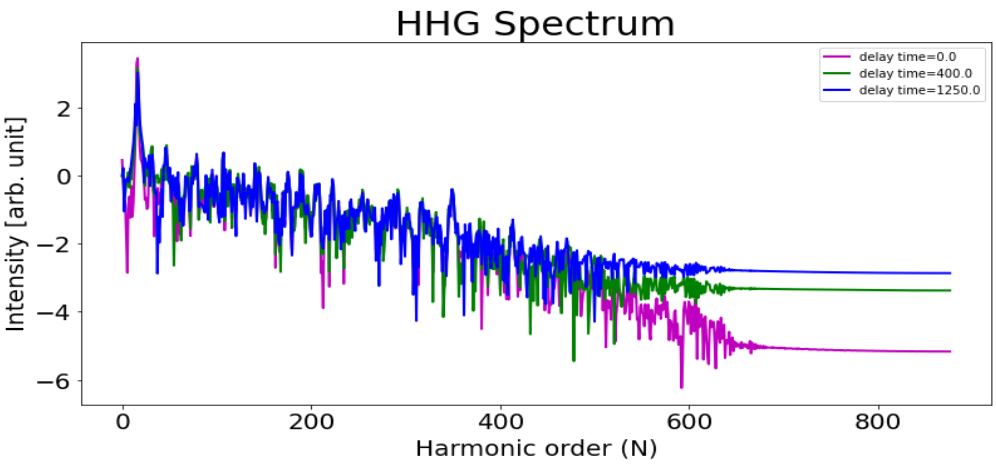

Fig 5:15 HHG Spectrum for Different Time Delays.

The **Fig 5:15** shows the HHG spectra for different time delays, 0.0a.u, 400a.u and 1250a.u, represented by Blue, Green and Purple colors, respectively. These are spectra with less grid points, 1600 points. However, with more grid points, say 4800, the plateau in **Fig 5:15** become well resolved. This is shown in **Fig 5:16** below.

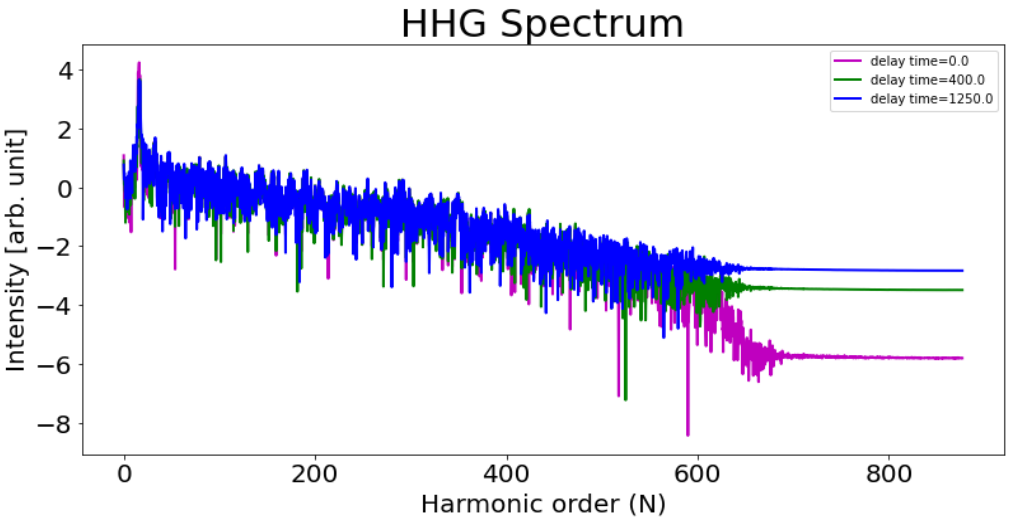

Fig 5:16 HHG Spectra for Different Time Delays.

Fig 5:15 and **Fig 5:16** show the HHG spectra for different time delays between the secondary and primary laser. The purple color shows the spectrum with a time delay of 0.0a.u while the green and the blue represent the HHG spectrum for 400 a.u. and 1250 a.u, time delays, respectively.

It is clearly seen in **Fig 5:16** that time delay causes some spectral shift on the spectrum. The longer the time delay the smaller the spectral shift.

Chapter6 Conclusions

In this thesis, I have investigated the High-order Harmonic Generation (HHG) process through laser atom interaction. Specifically, I used Hydrogen atom in: (i) a Single Infrared (IR) Laser field, (ii) a delayed double IR Laser field and (ii) a non-delayed double IR laser field. We indeed found that this HHG process can produce Extreme Ultraviolet (XUV) pulses which are in attoseconds timescale.

To achieve this goal, we played with different time delays between the two lasers in order to attempt to extend the cut off energy in the HHG spectra. This thesis clearly depicts how we can increase this cut off energy by using two replica IR which doubles the cut off energy compared to a single laser interacting with the Hydrogen atom H. With different delay time between the two pulses, harmonics of different orders are seen in the HHG spectrum. When lasers of intensities $2 \times 10^{14} \mathrm{W/cm^2}$ each interacts with H atom, the energy of emitted photons is of order 400 of the absorbed frequency which correspond to energy of 618eV. This frequency of recombination for a single laser and atom interaction is order of 78 which correspond to 120eV. This therefore clearly shows that double laser pulse interaction is so much higher compared to single laser pulse. The less the time delay, the more the cut off energy. This therefore can be transferred to practical implementation in the laser lab with available laser such as Ti-Sapphire (800nm). With more investment in the implementation, this analysis could be studied more by extending this research to other atoms like atoms like Argon. Also, effects of different time delay could be clearly seen by using Gabor transformation for the spectrum near the cut off region. Here in this thesis, it can only be seen that there is a spectral shift in intensity from the driving laser for different time delay between the driving and the secondary laser.

The challenge of this numerical analysis is the code implementation of the Gabor window of the cut off region for the HHG spectrum.

References

1. Kim, Dong Eon, et al. "For the extension of current attosecond pulses to multi-cycle driver regime and hard X-ray regime" **2009 IEEE LEOS Annual Meeting Conference Proceedings. IEEE** (2009)
2. Popmintchev, Tenio, et al. "The attosecond nonlinear optics of bright coherent X-ray generation" **Nature Photonics 4**, 822-832 (2010)
3. Gaarde, Mette B., and Kenneth J. Schafer. "Generating single attosecond pulses via spatial filtering" **Optics Letters 31**, 3188-3190 (2006)
4. Corder, Christopher, et al. "Development of a tunable high repetition rate XUV source for time-resolved photoemission studies of ultrafast dynamics at surfaces" **Laser Applications in Microelectronic and Optoelectronic Manufacturing (LAMOM) XXIII 10519**, SPIE (2018)
5. Sie, Edbert J., et al. "Time-resolved XUV ARPES with tunable 24–33 eV laser pulses at 30 meV resolution" **Nature communications 10**, 3535 (2019)
6. Chang, Zenghu. "Controlling attosecond pulse generation with a double optical gating" **Physical Review A 76**, 051403 (2007)
7. Herrmann, Daniel, et al. "Generation of sub-three-cycle, 16 TW light pulses by using noncollinear optical parametric chirped-pulse amplification" **Optics Letters 34**, 2459-2461 (2009)
8. Heyl, Christoph M., et al. "Scale-invariant nonlinear optics in gases" **Optica 3**, 75-81 9 (2016)
9. Corkum, P. áB, and Ferenc Krausz. "Attosecond science" **Nature Physics 3**, 381-387 (2007)
10. Feng, Ximao, et al. "Generation of isolated attosecond pulses with 20 to 28 femtosecond lasers" **Physical Review Letters 103**, 183901 (2009)
11. Pérez-Hernández, J. A., et al. "Extension of the cut-off in high-harmonic generation using two delayed pulses of the same colour." **Journal of Physics B: Atomic, Molecular and Optical Physics 42**, 134004 (2009)
12. Oldal, Lénárd Gulyás, et al. "All-Optical Experimental Control of High-Harmonic Photon Energy" **Physical Review Applied 16**, L011001 (2021)
13. Burnett, N. H., et al. "Harmonic generation in CO2 laser target interaction" **Applied Physics Letters 31**, 172-174 (1977)

14. Gould, R. Gordon. "The LASER, light amplification by stimulated emission of radiation" **The Ann Arbor conference on optical pumping, the University of Michigan 15**, 92 (1959)

15. Taylor, Nick. "LASER: The inventor, the Nobel laureate, and the thirty-year patent war". **Simon and Schuster**, (2002)

16. Grossmann, Frank. "Theoretical femtosecond physics: atoms and molecules in strong laser fields" **Springer** (2018)

17. Wang, Juan, et al. "Spatiotemporal variation in surface urban heat island intensity and associated determinants across major Chinese cities" **Remote Sensing 7**, 3670-3689 (2015)

18. Silfvast, William T. "Laser fundamentals" **Cambridge University Press**, (2004)

19. Chang, Zenghu. "Fundamentals of attosecond optics" **CRC Press**, (2016)

20. Feit, M. D., J. A. Fleck Jr, and A. Steiger. "Solution of the Schrödinger equation by a spectral method" **Journal of Computational Physics 47**, 412-433 (1982)

21. Csele, Mark. "Fundamentals of light sources and lasers" **John Wiley & Sons**, (2011)

22. Suhara, Toshiaki. "Semiconductor laser fundamentals" **CRC press**, (2004)

23. Silfvast, William T. "Laser Fundamentals Cambridge University Press" **New York, NY**, (1996)

24. Mahamood, Rasheedat Modupe, and R. M. Mahamood. "Laser basics and laser material interactions" **Laser Metal Deposition Process of Metals, Alloys, and Composite Materials,** 11-35 (2018)

25. Maiman, Theodore H., and Theodore H. Maiman. "Addendum 10: Reprint of TH Maiman, "Stimulated Optical Radiation in Ruby" **Nature 187**, 493–494 (2018)

26. Eckhardt, Gisela, et al. "Stimulated Raman scattering from organic liquids" **Physical Review Letters 9**, 455 (1962)

27. Paschotta, Rüdiger. "Rp photonics encyclopedia" **Available online: www. rp-photonics. com**, (2013)

28. Heckl, O. H., et al. "High harmonic generation in a gas-filled hollow-core photonic crystal fiber" **Applied Physics B 97**, 369-373 (2009)

29. Paul, Pierre-Marie, et al. "Observation of a train of attosecond pulses from high harmonic generation" **Science 292**, 1689-1692 (2001)

30. Haken, Hermann, et al. "Light and matter" **Springer Science & Business Media 5**, (2013)

31. Corkum, Paul, and Ferenc Krausz. "Attosecond science" **Nature physics 3**, 381-387 (2007)

32. Corkum, Paul B. "Plasma perspective on strong field multiphoton ionization" **Physical Review Letters 71**, 1994 (1993)

33. Nabekawa, Yasuo, et al. "Conclusive evidence of an attosecond pulse train observed with the mode-resolved autocorrelation technique" **Physical Review letters 96**, 083901 (2006)

34. Lewenstein, Maciej, et al. "Theory of high-harmonic generation by low-frequency laser fields" **Physical Review A 49**, 2117 (1994)

35. Ishikawa, Kenichi L., Eiji J. Takahashi, and Katsumi Midorikawa. "Wavelength dependence of high-order harmonic generation with independently controlled ionization and ponderomotive energy" **Physical Review A 80**, 011807 (2009)

36. Thyagarajan, K., and Ajoy Ghatak. "Laser fundamentals and applications" **Springer Science & Business Media**, (2010)

37. LeVeque, Randall J. "Finite difference methods for ordinary and partial differential equations: steady-state and time-dependent problems" **Society for Industrial and Applied Mathematics**, (2007)

38. Strikwerda, John C. "Finite difference schemes and partial differential equations" **Society for Industrial and Applied Mathematics**, (2004)

39. Ogundare, B. S. "On the pseudo-spectral method of solving linear ordinary differential equations." **Journal of Mathematics and Statistics 5**, 136 (2009)

40. Mazziotti, David A. "Spectral difference methods for solving the differential equations of chemical physics" **The Journal of chemical physics 117**, 2455-2468 (2002)

41. Doescher, S. W., and M. H. Rice. "Infinite square-well potential with a moving wall" **American Journal of Physics 37**, 1246-1249 (1969)

42. Cebeci, Tuncer. "Convective heat transfer" **Berlin: Horizons Pub**, (2002)

43. Crank, John, and Phyllis Nicolson. "A practical method for numerical evaluation of solutions of partial differential equations of the heat-conduction type" **Mathematical proceedings of the Cambridge philosophical society 43**, 1 (1947).

44. Shiner, A. D., et al. "Wavelength scaling of high harmonic generation efficiency" **Physical Review Letters 103**, 073902 (2009)

45. Pascal Diougue Ndione; "Ultrafast lasers interacting with Small Atoms, Research essay" **African Institute for Mathematical Science (AIMS)**, **Senegal** (2016)

46. Galloway, Benjamin R., et al. "High-Order Harmonic Generation Driven by Mid-Infrared Laser Light" **Diss. University of Colorado at Boulder**, (2017)

47. Feng, Ximao, et al. "Generation of isolated attosecond pulses with 20 to 28 femtosecond lasers" **Physical Review letters 103**, 183901 (2009)

48. Mashiko, Hiroki, et al. "Double optical gating of high-order harmonic generation with carrier-envelope phase stabilized lasers" **Physical Review letters 100**, 103906 (2008)

49. Vozzi, C. A. T. E. R. I. N. A., et al. "Characterization of a high-energy self-phase-stabilized near-infrared parametric source" **JOSA B 25**, B112-B117 (2008)

50. Krausz, Ferenc, and Misha Ivanov. "Attosecond physics" **Reviews of Modern Physics 81**, 163 (2009)

51. Lewenstein, Maciej, et al. "Theory of high-harmonic generation by low-frequency laser fields" **Physical Review A 49**, 2117 (1994)

52. Lan, Pengfei, et al. "Macroscopic effects for quantum control of broadband isolated attosecond pulse generation with a two-color field" **Physical Review A 79**, 043413 (2009)

53. Baltuška, Andrius, et al. "Attosecond control of electronic processes by intense light fields" **Nature 421**, 611-615 (2003)

54. Tate, J., et al. "Scaling of wave-packet dynamics in an intense midinfrared field" **Physical Review letters 98**, 013901 (2007)

55. Chen, Wenxiang, Guanglong Chen, and Dong Eon Kim. "Two-color field for the generation of an isolated attosecond pulse in water-window region" **Optics Express 19**, 20610-20615 (2011)

56. Mainfray, G., and G. Manus. "Multiphoton ionization of atoms" **Reports on Progress in Physics 54**, 1333 (1991)

57. Anatole Kenfack, "Introduction to Laser-Matter Interaction Lecture notes" **African University of Science and Technology [AUST], Nigeria**, (2018)

58. Jokanović, Vukoman, Dijana Trišić, and Marija Živković. "Review of lasers application in dentistry" **Stomatoloski Glasnik Srbije 67**, 36-49 (2020)

59. M. Lewenstein, P. Balcou, M. Y. Ivanov, A. L'Huillier, and P. B. Corkum, **Phys. Rev. A 49**, 2117 (1994)

60. Cam-Tu Le and Ngoc-Loan Phan J. Phys **Conf. Ser. 1506,** 012005 (2020)

61. Anh-Thu Le et al J. Phys. B: At. Mol **Opt. Phys 49**, 053001 (2016)

62. Pullen, M. G., et al. "Measurement of laser intensities approaching 10 15 W/cm 2 with an accuracy of 1%" **Physical Review A 87**, 053411 (2013)

63. P. Ehrenfest, Bemerkung ¨uber die angen¨aherte G¨**ultigkeit der klassischen Mechanik innerhalb der Quantenmechanik, Zeitschrift f¨ur Physik 45**, 7 (1927).

64. Torsten Leitner; “High order Harmonic Generation as a Possible Seed Source for the Bessey Free Electron Laser” **PhD Thesis submitted to Humboldt-Universitat zu Berlin**, (2007)